

# Gravitational wave generation by interaction of high power lasers with matter

## Part I: Shock wave model

Hedvika Kadlecová,<sup>1,\*</sup> Ondřej Klimo,<sup>1,2</sup> Stefan Weber,<sup>1</sup> and Georg Korn<sup>1</sup>

<sup>1</sup>*Institute of Physics of the ASCR, ELI-Beamlines project, Na Slovance 2, 18221, Prague, Czech Republic*

<sup>2</sup>*FNSPE, Czech Technical University in Prague, 11519 Prague, Czech Republic*

(Dated: December 3, 2024)

We analyze theoretical models of gravitational wave generation in the interaction of high power lasers with matter in linear approximation of gravitational theory. We derive the analytical formulas and estimates for the metric perturbations and the radiated power of the generated gravitational waves. Furthermore we investigate the characteristics of polarization and the behavior of test particles in the presence of gravitational wave which will be important for the detection.

PACS numbers: 52.38.-r, 04.30.Db, 52.27.Ey, 52.38.Kd

Keywords: gravitational waves, laser-plasma interaction

### I. INTRODUCTION

The direct detection of gravitational waves remained one of the biggest challenges of experimental physics since the original paper about their existence by Einstein in 1918 [1] till February 2016 when interferometer measurements on LIGO and VIRGO confirmed the prediction [2]. Their existence was indirectly shown thanks to the analytical work on radio pulses by Taylor and Hulse in 1974 who first recognized the pulsar PSR 1913+16 in a binary system [3]. The discovered pulsar was a unique binary pulsar which served as a perfect astrophysical laboratory for observations of very strong relativistic effects. The most important effect was the perpetual shortening of the rotational period of the two pulsars which experimentally proved Einstein's theory of general relativity. The theory predicts that the two pulsars approach each other on spiral trajectories while the binding energy is radiated away as gravitational waves. The theory predicted the shortening of 0,0758 ms per year and the measured value was  $0,0760 \pm 0,0005$  ms per year [4].

The motivation for today's expensive experiments is the understanding of the universe and strong astrophysical sources because the gravitational waves carry the properties of the original source. By their detection we can get obtain more information about the stars and the whole universe. The information is hidden in the direction, amplitude, frequency and polarization of gravitational waves. The recent detection will definitely open a new era of experimental physics and astronomy.

The greatest obstacle in the detection of gravitational waves is that their intensity is very weak compared to electromagnetic waves. The gravitational force is the weakest one in the universe but affects the mass effectively on large distances and dominates the physics processes in the universe. The ratio of the gravitational and electrostatic attraction forces between two electrons is  $10^{-42}$ . The other components of the radiation such as

electromagnetic one coming on Earth do not make the detection problem easier because they are much stronger than gravitational waves.

Gravitational waves can be detected by many techniques. They can be measured by change of lengths by extremely sensitive interferometers, piezoelectric crystals [5], superconductors, resonance chambers and by conversion of gravitational waves to electromagnetic waves by the Gertsenshtein effect [6, 7] or by sensors [8].

The first gravitational Hertz experiments were performed by Weber in the low frequency domain [9]. The Weber experiment constructed in 1960s consisted of a tube resonant detector. The detectors sensitivity was about  $h \approx 10^{-16}$  which is still smaller than the amplitude of gravitational waves coming from space on Earth which is about  $10^{-18}$ . The measurements made by Weber were not reproduced and it is assumed that some systematic mistake of the experiment was measured instead of gravitational waves. The work was followed by many groups. Today, the Weber type of detectors have sensitivities of  $< 10^{-19}$  for example at Louisiana university where they use two-mode superconducting transducer and amplifier (SQUID) in the frequency range  $< 100$  Hz. Other examples are the projects as MiniGrail [10] and Auriga in Padova (Italy) [11, 12].

The gravitational waves (GW) generated from astrophysical sources are searched for by large gravitational interferometer detectors such as the American LIGO [13, 14] and Italian- French VIRGO [15]. For a review see [16]. These detectors look for waves in the low frequency spectral band between 10 Hz to 20 kHz. The sensitivity of the LIGO type interferometers is about  $h = 10^{-23}$  which would allow to detect weak gravitational waves coming from supernova in our galaxy or Magellan Cloud. The experiments under construction are space-based interferometers, such as LISA [17] and DECIGO [18]. The vacuum environment would enable the interferometers to work without on Earth based noise. LISA would operate with  $h > 10^{-22}$  and in low frequency mode in mHz with launch on L3 ESA program in 2032. Other experiments in this area are GEO600 [19] and CEGO

---

\* Hedvika.Kadlecova@eli-beams.eu

(China) [20].

Recent interests in astrophysical sources of high frequency gravitational waves (HFGW) with frequencies  $\nu > 100$  kHz, GHz and higher lead to consider and review the so called GW Hertz experiment which consists of generation and detection of the GW signal in terrestrial laboratories.

The Hertz experiments in the high frequency domain were investigated by Chapline [21] and the well-known experimental group of Rudenko [22]. Namely, Rudenko suggested an experiment associated with high power electromagnetic waves and acoustic impulsive or shock waves travelling and interacting with a non-linear opto-acoustic media. Since lasers are the most powerful sources of electromagnetic radiation on Earth we can assume models where gravitational waves are produced by interaction of laser with mediums in different set ups as was suggested in [23, 24] for high power lasers like Peta Watt class lasers (PETAL [25], NIF-ARC [26]) and ELI [27]. The high intensity lasers would open a new prospects in their application into fundamental physics.

The main purpose of this paper is to correctly analyze the three generational models of high frequency gravitational waves (HFGW) in the interaction of high power laser pulse with matter. These models were suggested in [23, 24], from which we have chosen to investigate the shock wave model, shock wave model with ablation [28] and the piston model [29]. We investigate the polarization of the generated gravitational waves and the behavior of test particles in the gravitational field of the wave.

We suggest the generator type of gravitational wave experiment. The resulting perturbations of the waves are of magnitude about  $10^{-40}$  which is out of range of today's known detectors. The technology of detectors as interferometers or resonant chambers for low frequency gravitational waves is useless for the high frequency range and a different technology is required. The detection problem of the generated GW is not addressed in this paper. The feasibility of detection of waves in high frequency regime is discussed for example in [30] for X-ray lasers, their detection in microwave band was discussed in [7], detection by optically-levitated sensors with slightly higher frequency range than advanced LIGO was considered in [6].

In 2011, a new detection scheme was proposed, called Li-Baker detector of HFGW [31] which might have sensitivities  $10^{-32}$  at 10 GHz while the minimal detectable perturbation reaches  $10^{-37}$ . The detector is based on coupling between electromagnetic waves and GW in generalized inverse Gertsenshtein effect [32, 33].

The remainder of the paper is organized as follows. In Section II we review the basic theory of linearized gravity which we will use throughout the paper. We present the notation, the metric, the limitations of the theory, the analytical expression for perturbations and the luminosity, the polarization of the gravitational radiation and the test particles behavior in the slow motion and distant field approximation of the linearized gravitational theory.

In Section III, we review the assumed shock wave model of the experiment for the gravitational waves generation under laboratory conditions.

We derive the analytical formulas for the space perturbations and the luminosity of the gravitational radiation. For the specific data we derive the estimations for the experiment and measurement.

In Section IV we derive and analyze the polarization properties of the gravitational radiation and the different radiative properties with dependence on the orientation of the wave vector in the assumed shock wave model.

Section V concentrates on derivation and analysis of the behavior of the test particles in the field of passing gravitational waves in the presented shock wave model.

The main results are summarized in the concluding Section VI.

## II. LINEARIZED GRAVITATIONAL THEORY FOR GRAVITATIONAL WAVES STUDIES

In this section we review the linearized theory of gravitation [4, 34, 35] needed for the subsequent analysis. We will use it to set up the notation which will be analyzed throughout the paper according to [34].

### A. The basics of the theory

The linearized theory of gravitation assumes the existence of a coordinate system in spacetime where the metric is close to the Minkowski flat metric  $\eta_{\mu\nu}$

$$g_{\mu\nu} = \eta_{\mu\nu} + h_{\mu\nu}, \quad |h_{\mu\nu}| \ll 1, \quad (1)$$

where the perturbation of the metric  $h_{\mu\nu}$  has to be less than 1 in absolute value and its derivatives satisfy the same relationship. We want to solve the Einstein equations for the linearized metric (1),

$$R_{\mu\nu} - \frac{1}{2}g_{\mu\nu}R = \frac{8\pi G}{c^4}T_{\mu\nu}, \quad (2)$$

where  $G_{\mu\nu} = R_{\mu\nu} - \frac{1}{2}g_{\mu\nu}R$  is Einstein tensor composed from Ricci tensor  $R_{\mu\nu}$  and scalar curvature of the spacetime  $R$ ,  $T_{\mu\nu}$  is the stress-energy tensor,  $G$  is gravitational constant and  $c$  is the velocity of light. The equations simplify when we introduce

$$\bar{h}_{\mu\nu} = h_{\mu\nu} - \frac{1}{2}\eta_{\mu\nu}h. \quad (3)$$

The equations (2) then become

$$\square \bar{h}_{\mu\nu} + \eta_{\mu\nu} \partial^\rho \partial^\sigma \bar{h}_{\rho\sigma} - \partial^\rho \partial_\nu \bar{h}_{\mu\rho} - \partial^\rho \partial_\mu \bar{h}_{\nu\rho} = -\frac{8\pi G}{c^4}T_{\mu\nu}, \quad (4)$$

where  $\square = \frac{1}{c^2} \frac{\partial^2}{\partial t^2} - \Delta$  is the d'Alembert operator. Now, we use the gauge freedom to choose the Lorentz gauge

$$\partial^\nu \bar{h}_{\mu\nu} = 0, \quad (5)$$

to rewrite the Einstein equations (4) and we will get simple wave equation

$$\square \bar{h}_{\mu\nu} = -\frac{16\pi G}{c^4} T_{\mu\nu}. \quad (6)$$

We observe that the gauge freedom (5) gives four conditions which reduce the 10 independent components of the  $4 \times 4$  matrix  $h_{\mu\nu}$  to six independent components. The equations (5) and (6) imply the conservation of energy-momentum in linear theory for consistency,

$$\partial^\nu T_{\mu\nu} = 0. \quad (7)$$

### B. The TT gauge and polarization

We want to investigate the propagation of gravitational waves and their interaction with test particles (and therefore with their detector) therefore we are interested in the solutions of (6) outside of the sources

$$\square \bar{h}_{\mu\nu} = 0, \quad T_{\mu\nu} = 0. \quad (8)$$

We can further reduce the degrees of freedom to just two by gauge transformation. The metric perturbations will then be expressed in so called TT gauge (transversal and traceless). We will denote such a metric as

$$h_{\mu\nu} = h_{\mu\nu}^{TT}. \quad (9)$$

The tensor  $h_{\mu\nu}$  is purely spatial ( $h_{0\mu}$ ) and it is transverse to its own direction of propagation ( $h_{ij,j} = h_{ij}k_j = 0$ ) and is traceless ( $h_{kk} = 0$ ).

The two remaining degrees of freedom represent the two polarization modes of the gravitational wave which propagates with the speed of light  $c$ .

In the TT gauge, the spacetime components of Riemann curvature tensor

$$R_{j0k0} = R_{0j0k} = -R_{j00k} = -R_{0jk0}, \quad (10)$$

have simple form

$$R_{j0k0} = -\frac{1}{2} h_{jk,00}^{TT}, \quad (11)$$

the curvature tensor is gauge-invariant and it follows that  $h_{\mu\nu}$  can't have fewer components than it has in the TT gauge.

### C. The plane wave solution

We consider the simplest solution for the wave equation (6) which is the plane wave solution,

$$\bar{h}_{\mu\nu} = \text{Re} [A_{\mu\nu} \exp(ik_\alpha x^\alpha)], \quad (12)$$

where the  $A_{\mu\nu}$  amplitude and  $k_\mu$  wave vector satisfy  $k_\alpha k^\alpha = 0$ . The  $k_\alpha$  is a null vector and  $A_{\mu\nu} k^\alpha = 0$  so

that  $A_{\mu\nu}$  is orthogonal to  $k_\alpha$ . The solution describes a wave with frequency  $\omega/c \equiv k^0 = (k_x^2 + k_y^2 + k_z^2)^{1/2}$  which propagates with the speed of light in the direction  $(1/k^0(k_x, k_y, k_z))$ . The spatial components of perturbation metric  $h_{\mu\nu}^{TT}$  in TT gauge are obtained as

$$\bar{h}_{ij}^{TT} = \Lambda_{ij,kl} h_{kl}, \quad (13)$$

where

$$\Lambda_{ij,kl}(\hat{\mathbf{n}}) = P_{ik} P_{jl} - \frac{1}{2} P_{ij} P_{kl}. \quad (14)$$

The projector operator is  $P_{jk}(\hat{\mathbf{n}}) = \delta_{jk} - n_j n_k$  and  $n_k = k_k/k$  is the unit vector in the direction of propagation. Note that this projector method is valid only for plane waves, [4].

### D. The weak field sources with arbitrary velocity

The equations (6) can be solved using Green functions

$$\square_x G(\mathbf{x} - \mathbf{x}') = \delta^4(\mathbf{x} - \mathbf{x}'). \quad (15)$$

Then

$$\bar{h}_{ij}(t, \mathbf{x}) = -\frac{16\pi G}{c^4} \int d^4 x' G(\mathbf{x} - \mathbf{x}') T_{\mu\nu}(\mathbf{x}'). \quad (16)$$

We impose the boundary conditions for radiative problem which is solved by retarded Green functions

$$G(\mathbf{x} - \mathbf{x}') = -\frac{1}{4\pi |\mathbf{x} - \mathbf{x}'|} \delta(x_{ret}^0 - x'^0), \quad (17)$$

where  $x'^0 = ct$ ,  $x_{ret}^0 = ct_{ret}$ , and  $t_{ret} = t - \frac{|\mathbf{x} - \mathbf{x}'|}{c}$  is the retarded time. Then the solution of (6) is

$$h_{ij}^{TT}(t, \mathbf{x}) = \frac{4G}{c^4} \Lambda_{ij,kl}(\hat{\mathbf{n}}) \int d^4 x' \frac{1}{|\mathbf{x} - \mathbf{x}'|} T_{kl} \left( t - \frac{|\mathbf{x} - \mathbf{x}'|}{c}, \mathbf{x}' \right), \quad (18)$$

where  $\mathbf{x} = \hat{\mathbf{n}}$  and we will denote  $|\mathbf{x}| = r$  and use  $h_{ij}^{TT} = \Lambda_{ij,kl} h_{kl} = \Lambda_{ij,kl} \bar{h}_{kl}$ . The  $h_{ij}^{TT}$  depend only on spatial components of the integral  $T_{kl}$ . We denote the typical radius of the source  $d$ , and at  $r \gg d$  we expand

$$|\mathbf{x} - \mathbf{x}'| = r - \mathbf{x} \cdot \hat{\mathbf{n}} + O\left(\frac{d^2}{r}\right), \quad (19)$$

We are interested in the value of  $h_{ij}^{TT}$  at large distances from the source where the detector is located, therefore we take the limit  $r \rightarrow \infty$  at fixed time  $t$ . By this we obtain just the leading term which is  $\mathcal{O}(1/r)$  and we set  $|\mathbf{x} - \mathbf{x}'| = r$ . The remaining terms are  $\mathcal{O}(1/r^2)$  and we neglect them. The leading term reads at the large distances

$$h_{ij}^{TT}(t, \mathbf{x}) = \frac{4G}{r c^4} \Lambda_{ij,kl}(\hat{\mathbf{n}}) \int d^4 x' T_{kl} \left( t - \frac{r}{c} + \frac{\mathbf{x}' \cdot \hat{\mathbf{n}}}{c}, \mathbf{x}' \right). \quad (20)$$

Our convention for four-vector  $k^\mu = (\omega/c, \mathbf{k})$  and  $x^\mu = (ct, \mathbf{x})$  and then  $k_\mu x^\mu = -\omega t + \mathbf{k} \cdot \mathbf{x}$ .

### E. The low velocity multipole expansion

We assume the slow motion approximation of the source

$$v \ll c. \quad (21)$$

For such a non-relativistic motion the following relation is valid

$$\lambda \gg d, \quad (22)$$

where  $d$  is the source size. The wave length  $\lambda = \lambda/2\pi$  of the radiation generated is much bigger than the size of the system. If this condition is valid we do not need to know the internal motions of the source and therefore the radiation is dominated by the lowest multipole moments. To perform the multipole expansion we do Fourier transformation of  $T_{kl}$  in (20) for  $|x'| \leq d$  and then Taylor expansion of the exponential, and we get

$$T_{kl}(t - \frac{r}{c} + \frac{\mathbf{x}' \cdot \hat{\mathbf{n}}}{c}, \mathbf{x}') \simeq T_{kl}(t - \frac{r}{c}, \mathbf{x}') + \frac{x'^i n^i}{c} \partial_0 T_{kl} \quad (23)$$

$$+ \frac{1}{2c^2} x'^i x'^j n^i n^j \partial_0^2 T_{kl} + \dots, \quad (24)$$

which we can rewrite as general multipole expansion using the predefined moments as

$$h_{ij}^{TT}(t, \mathbf{x}) = \frac{1}{r} \frac{4G}{c^4} \Lambda_{ij,kl}(\hat{\mathbf{n}}) \times \left[ S^{kl} + \frac{1}{c} n_m \dot{S}^{kl,m} + \frac{1}{2c^2} n_m n_p \ddot{S}^{kl,mp} + \dots \right]_{ret} \quad (25)$$

where  $S^{kl} = \int d^3x T^{kl}(t, \mathbf{x})$  is a momentum of  $T^{ij}$  which can be expressed in terms of the two sets of energy moments ( $M, M^i, M^{ij}$ ) and moments of momentum density ( $P^i, P^{i,j}, P^{i,j,k}$ ). These two sets of moments have clear physical interpretation. The energy moments are defined as

$$\begin{aligned} M &= \frac{1}{c^2} \int d^3x T^{00}(t, \mathbf{x}), \\ M^i &= \frac{1}{c^2} \int d^3x T^{00}(t, \mathbf{x}) x^i, \\ M^{ij} &= \frac{1}{c^2} \int d^3x T^{00}(t, \mathbf{x}) x^i x^j, \end{aligned} \quad (26)$$

while the moments of momentum density read

$$\begin{aligned} P^i &= \frac{1}{c} \int d^3x T^{0i}(t, \mathbf{x}), \\ P^{i,j} &= \frac{1}{c} \int d^3x T^{0i}(t, \mathbf{x}) x^j, \\ P^{i,j,k} &= \frac{1}{c} \int d^3x T^{0i}(t, \mathbf{x}) x^j x^k. \end{aligned} \quad (27)$$

While the stress-energy tensor  $T_{\mu\nu}$  satisfies in linearized gravitational theory the condition (7) we can derive the relationships between those moments (26) and (27). For the lower orders of moments  $T^{00}$  we get

$$\begin{aligned} \dot{M} &= 0, \\ \dot{M}^i &= P^i, \end{aligned} \quad (28)$$

$$\dot{M}^{ij} = P^{i,j} + P^{j,i}, \quad (29)$$

and for moments  $T^{0i}$  we get

$$\begin{aligned} \dot{P}^i &= 0, \\ \dot{P}^{i,j} &= S^{ij}. \end{aligned} \quad (30)$$

We have denoted the derivative with respect to time as a dot over the quantity. We will use this notation throughout the text. The equations  $\dot{M} = 0$  and  $\dot{P}^i = 0$  are the conservation of mass and the conservation of the total energy-momentum of the source. From (29) and (30), using  $S^{ij} = S^{ji}$  we obtain

$$S^{ij} = \frac{1}{2} \dot{M}^{ij}. \quad (31)$$

We can continue for higher order moments like this but in our case we have enough information for our paper, for more details see [4, 34, 35].

Let us stress here that the lowest moment for gravitational waves is the quadrupole moment contrary to the electromagnetic waves where the lowest order is the dipole moment. Dipole moment vanishes because of the energy and momentum conservation law. In the following text we will work just in quadrupole approximation, i.e. the lowest term in the moment expansion (25).

### F. The mass and quadrupole moment, luminosity

The leading term in the expansion (25) using (31) is

$$[h_{ij}^{TT}(t, \mathbf{x})]_{\text{quad}} = \frac{1}{r} \frac{2G}{c^4} \Lambda_{ij,kl}(\hat{\mathbf{n}}) \ddot{M}^{kl}(t - r/c). \quad (32)$$

We introduce the quadrupole moment

$$\begin{aligned} I^{ij} &= M^{ij} - \frac{1}{3} \delta^{ij} M_{kk} \\ &\equiv \int d^3x \rho(t, \mathbf{x}) (x^i x^j - \frac{1}{3} r^2 \delta^{ij}), \end{aligned} \quad (33)$$

where  $\rho$  becomes the mass density ( in the lowest order in  $v/c$ ),

$$\rho = \frac{1}{c^2} T^{00}. \quad (34)$$

Then the mass moment can be rewritten as

$$M^{ij} = \int d^3x \rho(t, \mathbf{x}) x^i x^j. \quad (35)$$

The final expression for the metric perturbation which we will use is

$$[h_{ij}^{TT}(t, \mathbf{x})]_{\text{quad}} = \frac{1}{r} \frac{2G}{c^4} \Lambda_{ij,kl}(\hat{\mathbf{n}}) \ddot{I}^{kl}(t - r/c), \quad (36)$$

where we have used the property  $\Lambda_{ij,kl} \ddot{M}^{kl} = \Lambda_{ij,kl} (I^{kl} + \frac{1}{3} \delta^{kl} M_{rr})$  and the following is valid:  $\Lambda_{ij,kl} \delta^{kl} = 0$ .

The total gravitational luminosity (power) of the source in quadrupole approximation is

$$\mathcal{L}_{\text{quad}} = \frac{G}{5c^5} \langle \ddot{I}_{ij} \ddot{I}_{ij} \rangle, \quad (37)$$

where  $I_{ij}$  is evaluated in the retarded time  $t - r/c$ . Let us mention that the formula (37) is the famous quadrupole formula derived by Einstein.

In the following text, we are going to assume that the entities  $I_{ij}$  and  $h_{ij}^{TT}$  are evaluated in the retarded time. Another note concerns the lowering of the indices in the calculations. We use just the spatial metric to lower and rise the indices in the calculations, therefore the position of the indices in the tensors does not matter. The results would be different if we used the time component of the metric to lower and rise the indices.

### III. THE DERIVATION OF GRAVITATIONAL WAVE CHARACTERISTICS FOR GENERATIONAL SHOCK WAVE MODEL

This section is devoted to the derivation of fully analytical formulae of the luminosity  $\mathcal{L}_{GW}$  and the perturbation of the metric  $h_{GW}$  for the shock wave model using the linearized gravity theory from Section II. The results for ablation model and piston model will be presented in the Part II of this paper.

Partially, we will reproduce the results from the previous section and present semi-results which would be useful for calculations in the following sections.

#### A. The shock wave model

In this section we review the basic setup of the experiments for the generation of high frequency gravitational waves in the interaction of high power laser pulse with a medium as, suggested in [23, 24].

The first two models, shock wave and ablation model, were inspired by the work [28] where they study the planar laser-driven ablation. The process is a function of the laser intensity, wavelength, the target material, and the degree of inhibition of electron thermal conduction. The overall structure of the experiment is shown in Fig. 1.

In this configuration, the laser is interacting with a planar thick foil with more than  $100 \mu\text{m}$  thickness. The material is accelerated in the ablation zone and in the shock front. The points on the axis  $z_r$  and  $z_s$  indicate the spatial location where the gravitational waves start

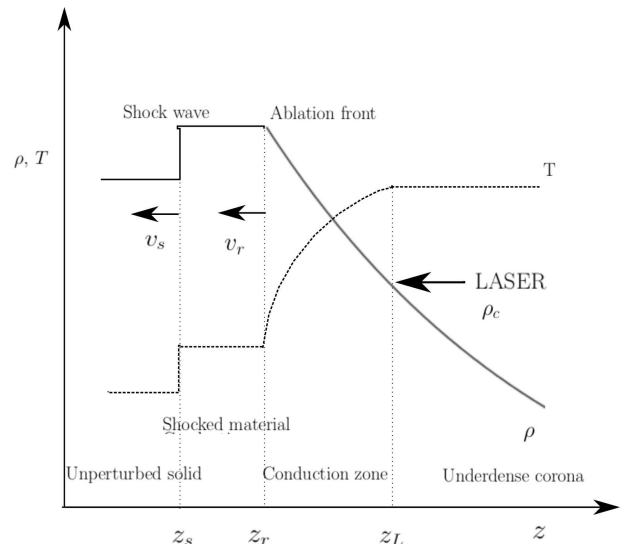


FIG. 1. The representation of density and temperature profiles for a typical laser heated planar target. The mass critical density is  $\rho_c = (M_i/Z)n_c$ .

to be generated. These two possibilities are divided into two separate models, the shock wave model and the ablation zone generation model. In the experiment, the two models are put together since each model represents one phase of the same experiment and therefore the radiation could be measured simultaneously.

The last model we are going to work with in the next paper is the piston model based on the idea of hole boring presented in [29]. The model is based on the dominant effect of radiation pressure on motion of particle in dense plasma at very high laser intensities  $I_L > 10^{20} \text{ W/cm}^2$ .

In the shock wave model, the laser launches a shock with the velocity  $v_s$ . The material from the foil is accelerated along the axis of motion  $z$  and it produces a change of mass – the change of quadrupolar mass moment of the source  $I_{ij}$ . A typical order of duration is 1 ns therefore the gravitational waves are generated in the GHz domain.

#### B. The limitations of the theory

Now, we will look for the limitations of the theory for the shock wave model experiment whether the low velocity limit (22) is satisfied for our experiments. The linear size of the source is more than  $d = 3.5 \mu\text{m} = 3.5 \times 10^{-6} \text{ m}$  and the reduced generated wavelength is  $\lambda = 4.7746 \times 10^{-2} \text{ m}$  for the gravitational wave length  $\lambda_g = 0.3 \text{ m}$ . The comparison (22) results into

$$3.5 \times 10^{-6} \ll 4.7746 \times 10^{-2} \implies 0.733 \times 10^{-4} \ll 1, \quad (38)$$

therefore the low velocity condition is still satisfied for our shock wave experiment. The same applies for the ablation model. The validity of this condition is weak

when we compare the validity of the condition (22) for neutron star, where the difference is  $10^{15}$ . To make the physics and calculations more valid we could calculate more moments in the moment expansion (25).

### C. The Shock wave model calculations

First, we will present the geometry of our experiment which will be similar for both models, the shock wave and ablation model. We assume a rectangular shape of the foil with parameters,  $a$ ,  $b$ ,  $l$ , and we choose the orthogonal coordinate system  $x$ ,  $y$ ,  $z$ . The parameter  $l$  is the thickness of the foil in the  $z$  direction. The distance of the laser and the detection point is  $z_L$ , Fig. (3). We assume the whole process takes place in the box of rectangular shape with parameters  $a, b, z_L$  for simplicity. The start of the coordinate system corresponds with the position where the detector would be possibly positioned.

The moving point where the density of the beam changes will be denoted as  $z_s$  with the functional dependence

$$z_s(t) = -v_s t + d, \quad (39)$$

where the shock wave velocity (strong shock is assumed) is defined as

$$v_s \simeq \sqrt{\frac{P_s}{\rho_0}}, \quad (40)$$

where  $P_s$  is ablation pressure and  $\rho_0$  is material density. We assume that for  $t = 0$ ,  $z_s(0) = d$ , therefore the constant in (39) is  $d = f_1 = f + l$  according to Figs. 3 and 2. In fact, the continuous motion is assumed for the shock wave. The whole calculation is made up to quadrupole moment in low velocity (non-relativistic) regime.

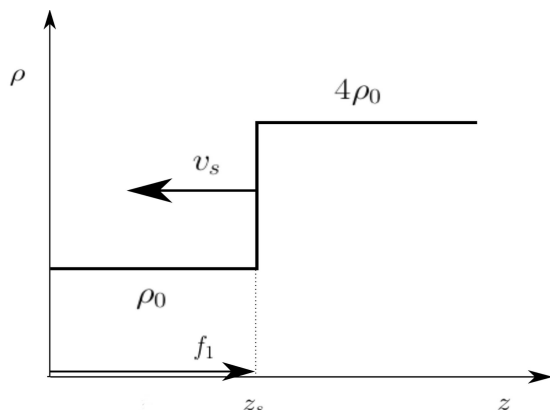


FIG. 2. The representation of density profile for the shock wave model.

In the following, we will calculate everything with general function  $z_s(t)$  and then we will substitute the explicit

function (39) at convenient places. General expressions might be useful for other forms of  $z_s(t)$ .

The basic input for the calculation is the density profile from Fig. 2. This is a detail from the Fig. 1 where one can see the jump in the density between the shocked material and the unperturbed solid part.

The step function for the density profile can be written as

$$\rho(\mathbf{x}) = \begin{cases} \rho_0 & \text{if } z < z_s, \\ 4\rho_0 & \text{if } z_s < z < z_L. \end{cases} \quad (41)$$

Better and more precise choice of the shock wave density would be  $\rho(\mathbf{x}) = 0$  for  $< 0, f >$  and  $< \frac{f+l-z_s}{4} + z_s >$ ,  $4\rho_0$  for  $< z_s, \frac{f+l-z_s}{4} + z_s >$  and  $\rho_0$  for  $< f, z_s >$ . The density (41) is idealization and gives the same main results thanks to the linear ansatz for  $z_s$ . The additional constants will vanish in derivations, subsequently, the perturbation  $h_{\mu\nu}$  and luminosity  $\mathcal{L}_{\text{quad}}$  will result in the same functional expressions up to a constant.

The first step in the calculation is the mass moment derivation.

#### 1. The mass moment

The mass moment (35) is a  $3 \times 3$  symmetric matrix in spacelike coordinates, therefore it is necessary to calculate just the components on diagonal  $M_{xx}, M_{yy}, M_{zz}$  and non-diagonal components  $M_{xy}, M_{yz}, M_{xz}$ .

The values for integration of the density (41) in (35) are  $x \in < 0, a >$ ,  $y \in < 0, b >$  and  $z \in < 0, z_L >$  which splits into  $< 0, z_s >$  and  $(z_s, z_L >$ . In other words, we integrate over the box in the Fig. 3. The mass moment diagonal components then read

$$\begin{aligned} M_{xx} &= Sa^2 \rho_0 \left( \frac{4}{3} z_L - z_s \right), \\ M_{yy} &= Sb^2 \rho_0 \left( \frac{4}{3} z_L - z_s \right), \\ M_{zz} &= S \rho_0 \left( \frac{4}{3} z_L^3 - z_s^3 \right), \end{aligned} \quad (42)$$

and the non-diagonal components  $M_{xy}, M_{yz}, M_{xz}$ ,

$$\begin{aligned} M_{xy} &= S^2 \rho_0 \left( z_L - \frac{3}{4} z_s \right), \\ M_{yz} &= Sb \rho_0 \left( z_L^2 - \frac{3}{4} z_s^2 \right), \\ M_{xz} &= Sa \rho_0 \left( z_L^2 - \frac{3}{4} z_s^2 \right). \end{aligned} \quad (43)$$

These semi-results will be useful for the polarization because it shows that it is sometimes more convenient to use the mass moment for calculations instead of the quadrupole moment.

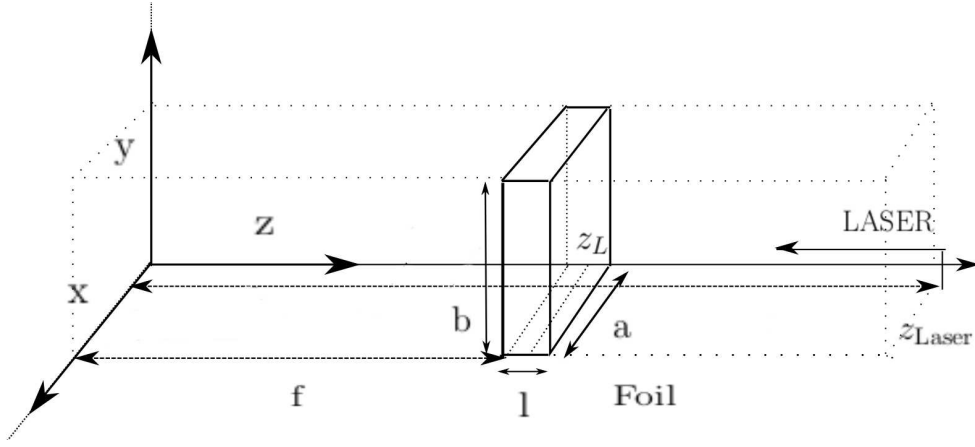


FIG. 3. The geometry set up for shock wave and ablation models at the start of the experiment. It shows our choice of the coordinate system, position of the foil and the laser. For purpose of calculations, we assume the area of experiment as a rectangular box with traversal parameters equal to the dimensions of the foil,  $x \in < 0, a \rangle$ ,  $y \in < 0, b \rangle$  where the  $z$ -coordinate of the box goes from the start of a coordinate system to the position of the laser,  $z \in < 0, z_L \rangle$ .

## 2. The quadrupole moment

The next step is the calculation of the quadrupole moment. We have to calculate the same components as for the mass moment since the quadrupole moment is symmetric matrix  $3 \times 3$  defined as (33). The second term is none-zero just for the diagonal components which will be more complicated. Then the non-diagonal components  $I_{xy}, I_{yz}, I_{xz}$  are

$$I_{xy} = M_{xy}, \quad I_{yz} = M_{yz}, \quad I_{xz} = M_{xz}. \quad (44)$$

The diagonal components  $I_{ii} = M_{ii} - \frac{1}{3}TrM$  read

$$\begin{aligned} I_{xx} &= \frac{S\rho_0}{3} \left\{ z_s^3 - (2a^2 - b^2)z_s + \frac{4}{3}z_L(2a^2 - b^2 - z_L^2) \right\}, \\ I_{yy} &= \frac{S\rho_0}{3} \left\{ z_s^3 - (2b^2 - a^2)z_s + \frac{4}{3}z_L(2b^2 - a^2 - z_L^2) \right\}, \\ I_{zz} &= \frac{S\rho_0}{3} \left\{ -2z_s^3 + (a^2 + b^2)z_s + \frac{4}{3}z_L(2z_L^2 - (a^2 + b^2)) \right\}. \end{aligned} \quad (45)$$

We observe that the diagonal components of quadrupole moment show cubic dependence on the function  $z_s$  and are missing a quadratic term. The non-diagonal components  $I_{yz}$  and  $I_{xz}$  are missing the linear dependence on  $z_s$ . When we substitute the function  $z_s(t)$  into  $I_{zz}$  component we will get the time dependency as

$$\begin{aligned} I_{zz} &= \frac{S\rho_0}{3} \left\{ 2v_s^3 t^3 - 6v_s^2 t^2 f_1 + v_s t (6f_1^2 - (a^2 + b^2)) \right. \\ &\quad \left. + f_1(a^2 + b^2) + \frac{4}{3}z_L(2z_L^2 - (a^2 + b^2)) \right\}. \end{aligned} \quad (46)$$

The quadrupole moment in the  $zz$  direction is given by a cubic polynomial in the duration of time  $t$  without the quadratic term. We observe that the authors [23, 24]

used just the most dominant term for their calculations. The other terms are new, the quadratic, linear and constant terms. The geometry of the setup influences the quadrupole moment from the quadratic term and lower. The derivatives of the quadrupole moment and mass moment are given in Appendix A, the derivatives with dependence on  $z_s$  in (A2) and with substitution of  $z_s$  in (A3).

## 3. The analytical form of perturbation and luminosity

Now, we calculate the components of the perturbation tensor according to (36) without projector appearing in (13). In other words, we obtain the components of the perturbation tensor in general form:

$$\begin{aligned} h_{xx} &= -\frac{2G}{3rc^4} S\rho_0 \left\{ (2a^2 - b^2)\ddot{z}_s - (z_s^3)'' \right\}, \\ h_{yy} &= -\frac{2G}{3rc^4} S\rho_0 \left\{ (2b^2 - a^2)\ddot{z}_s - (z_s^3)'' \right\}, \\ h_{zz} &= \frac{2G}{3rc^4} S\rho_0 \left\{ (a^2 + b^2)\ddot{z}_s - 2(z_s^3)'' \right\}, \end{aligned} \quad (47)$$

and the non-diagonal terms are

$$\begin{aligned} h_{xy} &= -\frac{3G}{2rc^4} S^2 \rho_0 \ddot{z}_s, \quad h_{xz} = -\frac{3G}{2rc^4} Sa\rho_0 (z_s^2)''', \\ h_{yz} &= -\frac{3G}{2rc^4} Sb\rho_0 (z_s^2)'''. \end{aligned} \quad (48)$$

By using the projector (14), we would obtain the perturbation tensor  $h_{\mu\nu}$  in TT calibration just for the special case of plane wave solution (12), see the next Section IV. The procedure of obtaining the  $TT$  calibration tensor is more complicated for more general waves [4].

The perturbation tensor with substitution of  $z_s(t)$

reads

$$h_{xx} = -\frac{4G}{rc^4}S\rho_0v_s^2(v_st - f_1), \quad h_{yy} = -\frac{4G}{rc^4}S\rho_0v_s^2(v_st - f_1),$$

$$h_{zz} = \frac{8G}{rc^4}S\rho_0v_s^2(v_st - f_1), \quad (49)$$

and the non-diagonal terms are

$$h_{xy} = 0, \quad h_{xz} = -\frac{3G}{rc^4}Sa\rho_0v_s^2, \quad h_{yz} = -\frac{3G}{rc^4}Sb\rho_0v_s^2, \quad (50)$$

where we used the derivatives of  $z_s$  listed in (A 1).

Now, we will look closely at the perturbation tensor. The diagonal components are the only time dependent components of the tensor, its components vanish for

$$f_1 = v_st, \quad (51)$$

which is the position of the detector.

The luminosity (37) reads just

$$\mathcal{L}_{\text{quad}} = \frac{G}{5c^5} \{ (\ddot{I}_{xx})^2 + (\ddot{I}_{yy})^2 + (\ddot{I}_{zz})^2 + 2(\ddot{I}_{xy})^2 + 2(\ddot{I}_{xz})^2 + 2(\ddot{I}_{yz})^2 \}. \quad (52)$$

After substituting the quadrupole moment components into (52), we get the general expression

$$\mathcal{L}_{\text{quad}} = \frac{G}{45c^5} S^2 \rho_0^2 \{ 6[(z_s^3)''']^2 - 6\ddot{z}_s(z_s^3)''(a^2 + b^2) + (\ddot{z}_s)^2[(a^2 + b^2)^2 + (2a^2 - b^2)^2 + (2b^2 - a^2)^2] + \frac{81}{8}S^2 \} + \frac{81}{8}(a^2 + b^2)[(z_s^2)''']^2 \}. \quad (53)$$

The explicit substitution  $z_s$  simplifies the expression (52) that just the diagonal components of quadrupole moment contribute to the result, see (A12). The expression (53) further simplifies to

$$\mathcal{L}_{\text{quad}} = \frac{24G}{5c^5} S^2 \rho_0^2 v_s^6. \quad (54)$$

Finally, we will use the explicit expression for the velocity  $v_s$  via (40). Here, we will use more general expression for  $P_s$  which will allow us to have control over more parameters than the one used in [23, 24] for a fixed wavelength. The relation of  $P_s$  and  $I_L$  is the following, [36],

$$P_s = R_t^{1/3} I_L^{2/3}, \quad (55)$$

$R_t$  denotes the target 'density' as

$$R_t = \frac{1}{2} \frac{A}{Z} m_p n_c, \quad (56)$$

and  $n_c$  is the critical density defined as

$$n_c = \frac{\epsilon_0 m_e (2\pi c)^2}{e^2 \lambda_L^2}, \quad (57)$$

where  $\epsilon_0$  is vacuum permittivity of vacuum,  $m_e$  is the rest mass of the electron,  $e$  is the charge of electron and  $\lambda_L$  is the wave length of the laser. All of the parameters in (57) are constants except the laser wavelength  $\lambda_L$  which is constant given by the specific experiment. We will keep the constant  $R_t$  in general form till substituting some explicit values.

After inserting (40) and (55), we will obtain the final expression for luminosity of gravitational radiation,

$$\mathcal{L}_{\text{quad}} = \frac{24}{5} \frac{G}{c^5} \frac{R_t}{\rho_0} P_L^2, \quad (58)$$

where we have used the power definition as

$$P_L = S I_L. \quad (59)$$

The luminosity then depends on the power of the laser, the density of the material and the laser wavelength. The numerical factor in front of the fraction for estimation will be presented in the next subsection.

The perturbation component  $h_{zz}^{GW}$  becomes using (40), (55) and (59),

$$h_{zz} = \frac{8G}{rc^4} \left( \left( \frac{R_t}{\rho_0} \right)^{1/2} E_L - S f_1 R_t^{1/3} I_L^{2/3} \right), \quad (60)$$

where we used the energy of the laser,

$$E_L = S I_L t. \quad (61)$$

This is the final formula for the perturbation of the space by gravitational wave in the  $zz$  direction. When we compare our result with the ones in [23, 24] we observe that the first term in the brackets generalizes the result with the  $R_t$  dependency. The value of the perturbation decreases with the distance as  $1/r$  and will be zero at infinity. We have obtained additional constant term which reduces the first term in the brackets. The numerical factors will be evaluated in the next subsection for specific values for an experiment.

Just for curiosity, lets have a look at the quadrupole moment, how it will look after using (40), (55) and (61),

$$I_{zz}(t) = \frac{\rho_0}{3} \left\{ -2 \frac{R_t^{1/2} E_L}{\rho_0^{3/2}} t^2 + (a^2 + b^2) \frac{S(R_t^{1/2} I_L)^{1/3}}{\sqrt{\rho_0}} t + \frac{4}{3} S L (2z^2 - (a^2 + b^2)) \right\}. \quad (62)$$

The expression is a quadratic function of the length of the laser pulse  $t$ , the quadratic coefficient is given by  $E_L$  and the material density  $\rho_0$  and  $R_t$  which depends on the wave length of laser  $\lambda_L$ , the linear coefficient is given by the intensity of the laser  $I_L$ , material density  $\rho_0$  and  $R_t$  dependent on  $\lambda_L$  and geometry of the setup,  $a, b, z_L$  and  $f_1$ .

4. *The estimations for the  $h_{\mu\nu}$  and  $\mathcal{L}_{quad}$  for real experiment*

We will evaluate the numerical factors in final results for luminosity (58) and the perturbation  $h_{zz}^{GW}$  of the space by the gravitatonal wave in  $zz$  direction, (60), which will be useful for real experiment.

Now, we arrive to the expression for the luminosity as

$$\mathcal{L}_{quad}\left[\frac{erg}{s}\right] = 1.34051 \times 10^{-25} \left[\frac{s^3}{g\text{ cm}^2}\right] \frac{R_t[\text{kg}/\text{m}^3]}{\rho_0[\text{g}/\text{cm}^3]} P_L^2[\text{PW}]. \quad (63)$$

When we compare our result with [23, 24] we observe that our estimation is six orders lower. Additionally, we have used general expression (52) for derivation of the result.

Next, we will perform the estimation for the  $zz$  component of the perturbation tensor  $h_{ij}$ . First, we will investigate the first time dependent physical part of (60). Similarly to the previous case, we obtain

$$h_{zz} = 6.68 \times 10^{-37.5} \left[\frac{s^2}{\text{kg m}}\right] \frac{1}{r[\text{cm}]} \left(\frac{R_t[\text{kg}/\text{m}^3]}{\rho_0[\text{g}/\text{cm}^3]}\right)^{1/2} E_L[\text{MJ}]. \quad (64)$$

The second constant term is a new contribution to the result which depends on the geometry of the setup and the choice of  $f_1$ ,

$$h_{zz}^{const} = -6.68 \times 10^{-35.3} \left[\frac{s^2}{\text{kg m}}\right] \frac{S[\text{cm}^2] f_1[\text{cm}]}{r[\text{cm}]} R_t^{1/3} \left[\frac{\text{kg}}{\text{m}}\right]^{1/3} \times I_L^{2/3} \left[\frac{\text{PW}}{\text{cm}^2}\right]^{2/3}. \quad (65)$$

This constant term has no physical meaning because we can make it zero by choosing different center of coordinate system with start at  $d = f_1 = 0$ .

The value of  $R_t$  can be estimated either, we have chosen Carbon as a material for the target with  $A = 12$ ,  $Z = 6$  and wavelength  $\lambda_L = 0.35 \times 10^{-4}$  cm. While using standard constants in (56) and (57), we will obtain

$$R_t = 15.144[\text{kg}/\text{m}^3]. \quad (66)$$

For experimental values we will evaluate our expressions

$$\begin{aligned} P_L &= 0.5 \text{ PW}, & \rho_0 &= 30 \text{ mg}/\text{cm}^3, & E_L &= 0.5 \text{ MJ}, \\ \tau &= 1 \text{ ns}, & \lambda_L &= 300 \mu\text{m}, \end{aligned} \quad (67)$$

and the detection distance is  $R = 10$  m or equivalently  $f_1 = f = 10$  m, parameters  $a, b$  of the target foil are  $a = b = 1 \mu\text{m} = 10^{-4}$  cm and therefore  $I_L = 0.5 \times 10^8 [\text{PW}/\text{cm}^2]$ . The outgoing gravitational radiation has frequency  $\nu_g = 1$  GHz and wave length  $\lambda_g = 0.3$  m. The final estimations for our expressions of the luminosity and the perturbation are:

$$\begin{aligned} \mathcal{L}_{GW} &\simeq 1.69172 \times 10^{-23} [\text{erg}/\text{s}], \\ h_{zz}^{GW} &\simeq 2.373 \times 10^{-39}. \end{aligned} \quad (68)$$

The orders of the first term of  $h_{zz}$  correspond to [23, 24] but the order of  $\mathcal{L}_{GW}$  is four orders lower.

Interestingly, the constant term (65) results in the estimation to a number  $h_{zz}^{const} = -1.12419 \cdot 10^{-37}$  which is two orders higher then (68). This term is of coordinate nature and can be transformed away therefore has no physical meaning.

We have derived and investigated generalized formulae for the luminosity (63) and the perturbation tensor  $h_{zz}$  (64) which newly depends on the laser wavelegh  $\lambda_g$  through  $R_t$ . The resulting estimations for specific experimental values agree with aformentioned [23, 24].

#### IV. THE POLARIZATION OF GRAVITATIONAL WAVES

In this section, we are going to investigate the two polarization modes of the gravitational waves which are generated by the models. We derive the amplitudes of the gravitational wave in two independent modes, + and -, and focus on their interpretation which would be useful for real experiment conditions.

The plane wave solution can be rewritten as

$$h_{ij}^{TT}(x) = A_{ij} e^{i\mathbf{k}\cdot\mathbf{x}}, \quad (69)$$

where  $A_{ij}$  is the amplitude of the gravitatonal wave, the solution depends on the wave vector  $k^\mu = (\omega/c, \mathbf{k})$  and  $\omega/c = |\mathbf{k}|$  and  $\mathbf{k} \cdot \mathbf{x} = k_\sigma x^\sigma$ . This result is valid for one plane wave or for the superposition of plane waves with different frequencies but with the same direction of propagation  $\mathbf{n} = \mathbf{k}/|\mathbf{k}|$ . The wave is truly transversal since  $h_{ij}^{TT} k_j = 0$ .

We get the components of  $h_{ij}^{TT}$  in  $TT$  gauge in spatial coordinates  $h_{i\mu\nu}$  as

$$h_{ij}^{TT}(x) = \Lambda_{ij,kl} h_{kl}, \quad (70)$$

where the projector dependent on the general direction of propagation  $\mathbf{n}$  takes the form

$$\begin{aligned} \Lambda_{ij,kl}(\mathbf{n}) &= \delta_{ik} \delta_{jl} - \frac{1}{2} \delta_{ij} \delta_{kl} - n_j n_l \delta_{ik} - n_i n_k \delta_{jl} \\ &+ \frac{1}{2} n_k n_l \delta_{ij} + \frac{1}{2} n_i n_j \delta_{kl} + \frac{1}{2} n_i n_j n_k n_l. \end{aligned} \quad (71)$$

We can decompose the gravitational wave into two linearly polarized components or into two circularly polarized components. To decompose the gravitational wave into two independent linearly polarized waves we can rewrite the polarization tensor in (70) as

$$h_{ij}^{TT}(x) = h_{+ij} + h_{\times ij}, \quad (72)$$

where we can introduce unit linear tensors of linear polarization as

$$\begin{aligned} e_{+ij} &= (\mathbf{e}_1)_i (\mathbf{e}_1)_j - (\mathbf{e}_2)_j (\mathbf{e}_2)_i, \\ e_{\times ij} &= (\mathbf{e}_1)_i (\mathbf{e}_2)_j + (\mathbf{e}_1)_j (\mathbf{e}_2)_i. \end{aligned} \quad (73)$$

We have denoted  $\mathbf{e}_1$  and  $\mathbf{e}_2$  as unit vectors.

The two independent linearly polarized waves can be written as

$$h_{+ij} = A_+ e^{-i\omega(t-\mathbf{n}\cdot\mathbf{x})} e_{+ij}, \quad (74)$$

$$h_{\times ij} = A_\times e^{-i\omega(t-\mathbf{n}\cdot\mathbf{x})} e_{\times ij}, \quad (75)$$

where  $A_+$  and  $A_-$  are amplitudes of the two independent polarizations.

For example  $\mathbf{e}_1 = (1, 0, 0)$  and  $\mathbf{e}_2 = (0, 1, 0)$  for the wave vector  $\mathbf{n} = (0, 0, 1)$  we will get the result for wave propagation in  $z$  coordinate.

We can investigate the gravitational waves with dependence on the direction of the propagation, i.e. on the wave vector. The set up of our models is that the direction of the motion is the  $z$  coordinate. Therefore it makes sense to study the wave vectors oriented in the transversal directions  $x, y$ . Then we look at the general orientation of the wave vector in spherical coordinates and analyze the space distribution of the gravitational waves from the experiment. These results could help in specifying the exact position for detectors in experiment to measure non-zero values.

### A. The $x, y$ and $z$ directions of the wave vector

First, we are going to investigate the gravitational perturbations in the direction of the propagation, in the  $z$ -coordinate.

#### 1. The wave propagation in the $z$ -direction

The  $h_{ij}^{TT}$  (70) has then the only non-vanishing components as

$$\begin{aligned} h_{xx}^{TT} &= -h_{yy}^{TT} = \text{Re} \left\{ A_+ e^{-i\omega(t+z/c)} \right\}, \\ h_{xy}^{TT} &= h_{yx}^{TT} = \text{Re} \left\{ A_\times e^{-i\omega(t+z/c)} \right\}, \end{aligned} \quad (76)$$

for the wave propagation vector in the  $z$ -direction  $n = (0, 0, -1)$ . We have used the definition of perturbation tensor (32) expressed conveniently with the mass moment together with the only non-zero components of the projector  $\Lambda_{ij,kl}$  (71),

$$\begin{aligned} \Lambda_{xx,xx} &= \Lambda_{yy,yy} = \frac{1}{2}, & \Lambda_{yy,xx} &= \Lambda_{xx,yy} = -\frac{1}{2}, \\ \Lambda_{xy,xy} &= \Lambda_{yx,yx} = 1. \end{aligned} \quad (77)$$

Generally the  $h_{ij}^{TT}$  can be summarized as

$$h_{ij}^{TT} = \text{Re} \left\{ \begin{pmatrix} A_+ & A_\times & 0 \\ A_\times & -A_+ & 0 \\ 0 & 0 & 0 \end{pmatrix}_{ij} e^{-i\omega(t+z/c)} \right\}, \quad (78)$$

where  $A_+$  and  $A_\times$  represent two independent orthogonal modes of polarization and  $ij$  are spatial indices.

The waves are therefore linearly polarized in the direction of propagation, this follows from the comparison of (76) and the definitions of linear decomposition of gravitational wave (72). We obtain the amplitudes of the polarization modes for the shock wave model in the form, [34],

$$A_+ = \frac{1}{r} \frac{G}{c^4} (\ddot{M}_{xx} - \ddot{M}_{yy}), \quad (79)$$

$$A_\times = \frac{2}{r} \frac{G}{c^4} \ddot{M}_{xy}. \quad (80)$$

Then we use the mass moments expressed in terms of derivatives of function  $z$ , the amplitudes read as follows,

$$A_+ = \frac{1}{r} \frac{G}{c^4} S \rho_0 \ddot{z}_s (b^2 - a^2), \quad (81)$$

$$A_\times = -\frac{3}{2r} \frac{G}{c^4} S^2 \rho_0 \ddot{z}_s. \quad (82)$$

When we substitute the ansatz for the velocity  $z_s$  (39) and its derivatives (A2), we observe that

$$A_+ = A_\times = 0. \quad (83)$$

Therefore the radiation  $h_{ij}^{TT}$  is vanishing for the orientation of the wave vector into the direction of motion of the experiment. The waves do not radiate along the  $z$  axis in which the motion occurs.

The result corresponds to the case of quadrupole oscillator example of two mass particles which are connected by a spring oriented in the  $z$  direction [35]. In the next section, we will observe that this is just a consequence of the geodesic deviation equation (128). The gravitational wave is not just transversal mathematically, i.e.  $h_{ij}^{TT}$ , but it has its physical effects. The gravitational radiation is non-zero in the other directions, for example in the direction of the  $x$  and  $y$  axes, see the next subsections.

#### 2. The wave propagation in the $x$ -direction

The  $h_{ij}^{TT}$  (70) has the only non-vanishing components for the wave vector in the  $x$ -direction  $n = (1, 0, 0)$ ,

$$\begin{aligned} h_{yy}^{TT} &= -h_{zz}^{TT} = \text{Re} \left\{ A_+ e^{-i\omega(t-x/c)} \right\}, \\ h_{zy}^{TT} &= h_{yz}^{TT} = \text{Re} \left\{ A_\times e^{-i\omega(t-x/c)} \right\}, \end{aligned} \quad (84)$$

where we have used again the definition of perturbation tensor (32) together with the only non-zero components of the projector  $\Lambda_{ij,kl}$  (71)

$$\begin{aligned} \Lambda_{yy,yy} &= \Lambda_{zz,zz} = \frac{1}{2}, & \Lambda_{zz,yy} &= \Lambda_{yy,zz} = -\frac{1}{2}, \\ \Lambda_{zy,zy} &= \Lambda_{yz,yz} = 1. \end{aligned} \quad (85)$$

The non-vanishing components of  $h_{ij}^{TT}$  can be rewritten as

$$h_{ij}^{TT} = \text{Re} \left\{ \begin{pmatrix} 0 & 0 & 0 \\ 0 & A_+ & A_\times \\ 0 & A_\times & -A_+ \end{pmatrix}_{ij} e^{-i\omega(t-x/c)} \right\}. \quad (86)$$

The waves are linearly polarized as in the previous case. We obtain the amplitudes of the polarization modes as, [34]:

$$A_+ = \frac{1}{r} \frac{G}{c^4} (\ddot{M}_{yy} - \ddot{M}_{zz}), \quad (87)$$

$$A_\times = \frac{2}{r} \frac{G}{c^4} \ddot{M}_{yz}. \quad (88)$$

Then we use the mass moments expressed in terms of derivatives of function  $z_s$ , the amplitudes read as follows,

$$A_+ = -\frac{1}{r} \frac{G}{c^4} S \rho_0 [b^2 \ddot{z}_s - (z_s^3)''], \quad (89)$$

$$A_\times = -\frac{3}{2r} \frac{G}{c^4} S \rho_0 b (z_s^2)'' \quad (90)$$

After we use the ansatz for the  $z_s$  we get

$$A_+ = \frac{6}{r} \frac{G}{c^4} S \rho_0 v_s^2 (f_1 - v_s t), \quad (91)$$

$$A_\times = -\frac{3}{r} \frac{G}{c^4} S \rho_0 b v_s^2. \quad (92)$$

We have obtained non-zero amplitudes for both '+' and '×' polarization modes. The amplitudes depend on the focus area  $S$ , the density of the material  $\rho_0$  and the velocity of the ions  $v_s$ . The amplitudes vanish as the radial distance  $r \rightarrow \infty$  and it decreases like  $1/r$ .

Importantly, the amplitude of the '+' polarization is linearly time dependent and the other one × is not. The time when  $A_+$  vanishes is  $t_{det} = f_1/v_s$  is a time when the radiation reaches the detector. This fact will be investigated in more detail in the section where we will deal with the influence of the wave on test particles (V).

The amplitudes of radiation and the radiative characteristics of the radiation are the main results of this paper.

### 3. The wave propagation in the $y$ -direction

The last direction we are going to investigate is the  $y$ -direction transversal to the direction of motion in  $z$ -coordinate. The perturbation tensor in  $TT$  calibration (70) for the wave vector in the  $y$ -direction  $n = (0, 1, 0)$  reads

$$\begin{aligned} h_{xx}^{TT} &= -h_{zz}^{TT} = \text{Re} \left\{ A_+ e^{-i\omega(t-y/c)} \right\}, \\ h_{zx}^{TT} &= h_{xz}^{TT} = \text{Re} \left\{ A_\times e^{-i\omega(t-y/c)} \right\}, \end{aligned} \quad (93)$$

where we have used again the definition of perturbation tensor (32) expressed conveniently with the mass moment together with the only non-zero components of the projector  $\Lambda_{ij,kl}$  (71)

$$\begin{aligned} \Lambda_{xx,xx} &= \Lambda_{zz,zz} = \frac{1}{2}, & \Lambda_{zz,xx} &= \Lambda_{xx,zz} = -\frac{1}{2}, \\ \Lambda_{zx,zx} &= \Lambda_{xz,xz} = 1. \end{aligned} \quad (94)$$

We can summarize the non-vanishing components of  $h_{ij}^{TT}$  as

$$h_{ij}^{TT} = \text{Re} \left\{ \begin{pmatrix} A_+ & 0 & A_\times \\ 0 & 0 & 0 \\ A_\times & 0 & -A_+ \end{pmatrix}_{ij} e^{-i\omega(t-y/c)} \right\}. \quad (95)$$

Again, the waves are linearly polarized as in the previous cases. The amplitudes of the polarization modes become, [34]:

$$A_+ = \frac{1}{r} \frac{G}{c^4} (\ddot{M}_{xx} - \ddot{M}_{zz}), \quad (96)$$

$$A_\times = -\frac{2}{r} \frac{G}{c^4} \ddot{M}_{xz}. \quad (97)$$

Then when using the mass moments expressed in terms of derivatives of function  $z_s$ , the amplitudes read as follows,

$$A_+ = -\frac{1}{r} \frac{G}{c^4} S \rho_0 [a^2 \ddot{z}_s - (z_s^3)''], \quad (98)$$

$$A_\times = \frac{3}{2r} \frac{G}{c^4} S \rho_0 a (z_s^2)'' \quad (99)$$

After we use the ansatz for the  $z_s$  we get

$$A_+ = \frac{6}{r} \frac{G}{c^4} S \rho_0 v_s^2 (f_1 - v_s t), \quad (100)$$

$$A_\times = \frac{3}{r} \frac{G}{c^4} S \rho_0 a v_s^2. \quad (101)$$

The resulting amplitudes  $A_+$  and  $A_-$  have the form as in the direction  $x$  (91) and (92) apart from the sign in  $A_\times$ . Importantly, the  $A_+$  amplitude depends linearly on time and again the other one  $A_\times$  is constant in time. The results have the same character as in the previous case. The amplitudes vanish as the radial distance  $r \rightarrow \infty$  and decrease as  $1/r$ , the amplitude  $A_+$  vanishes for time  $t_{det} = f_1/v_s$  when the radiation reaches the detector.

Finally, we are going to investigate the amplitudes with the general wave vector of propagation.

## B. The general direction of the wave vector

The general direction of the wave propagation can be expressed in the spherical coordinates as

$$n = (\sin \theta \sin \phi, \sin \theta \cos \phi, \cos \theta), \quad (102)$$

and the perturbation tensor can be obtained via (32) and the projector (71).

The general expressions for the two modes of polariza-

tions are, [34],

$$A_+(t; \theta, \phi) = \frac{1}{r} \frac{G}{c^4} \left[ \ddot{M}_{xx} (\cos^2 \phi - \sin^2 \phi \cos^2 \theta) \right. \\ + \ddot{M}_{yy} (\sin^2 \phi - \cos^2 \phi \cos^2 \theta) - \ddot{M}_{zz} \sin^2 \theta \\ - \ddot{M}_{xy} \sin 2\phi (1 + \cos^2 \theta) + \ddot{M}_{xz} \sin \phi \sin 2\theta \\ \left. + \ddot{M}_{yz} \cos \phi \sin 2\theta \right], \quad (103)$$

$$A_\times(t; \theta, \phi) = \frac{1}{r} \frac{G}{c^4} \left[ (\ddot{M}_{xx} - \ddot{M}_{yy}) \sin 2\phi \cos \theta \right. \\ + 2\ddot{M}_{xy} \cos 2\phi \cos \theta - 2\ddot{M}_{xz} \cos \phi \sin \theta \\ \left. + 2\ddot{M}_{yz} \sin \phi \sin \theta \right], \quad (104)$$

and the whole components of  $h_{ij}^{TT}$  can be expressed as (72) and (74, 75). Afterwards we use the mass moments expressed in terms of derivatives of function  $z_s$ , the amplitudes read as follows,

$$A_+(t; \theta, \phi) = \frac{3}{4r} \frac{G}{c^4} S \rho_0 \left[ \frac{4}{3} (z_s^3)'' \sin^2 \theta \right. \\ \left. - (z_0^2)'' \sin 2\theta (a \sin \phi + b \cos \phi) \right], \quad (105)$$

$$A_\times(t; \theta, \phi) = \frac{3}{2r} \frac{G}{c^4} S \rho_0 (z_s^2)'' \sin \theta (a \cos \phi - b \sin \phi). \quad (106)$$

After we use the ansatz for the  $z_s$ , we get

$$A_+(t; \theta, \phi) = \frac{3}{2r} \frac{G}{c^4} S \rho_0 v_s^2 [4(f_1 - v_s t) \sin^2 \theta \\ - \sin 2\theta (a \sin \phi + b \cos \phi)], \quad (107)$$

$$A_\times(t; \theta, \phi) = \frac{3}{r} \frac{G}{c^4} S \rho_0 v_s^2 \sin \theta (a \cos \phi - b \sin \phi). \quad (108)$$

We obtained the amplitudes of two independent polarization modes with the general wave vector of propagation. The character of the amplitudes resembles the results from the two previous cases, the amplitude  $A_+$  is linearly time dependent and the  $A_\times$  is constant in time. The amplitudes vanish as the radial distance  $r \rightarrow \infty$  and decreases as  $1/r$ .

We will obtain the three previous cases as subcases of these general amplitudes. The case  $\mathbf{n} = z$  (IV A 1) for  $\theta = 0^\circ$ ,  $\phi = 0^\circ$ , the case  $\mathbf{n} = x$  (IV A 2) can be obtained for  $\theta = 90^\circ$ ,  $\phi = 90^\circ$  and case  $\mathbf{n} = y$  (IV A 3) for  $\theta = 90^\circ$ ,  $\phi = 0^\circ$ .

To visualize the amplitudes it is convenient to rewrite them as

$$A_+(t; \theta, \phi) = \frac{3}{2} \frac{G}{c^4} S \rho_0 v_s^2 P_{A_+}(\theta, r), \\ A_\times(t; \theta, \phi) = \frac{3G}{c^4} S \rho_0 v_s^2 P_{A_\times}(\theta, r), \quad (109)$$

where the angular dependence is denoted as

$$P_{A_+}(\theta, r) = \frac{1}{r} \{4(f_1 - v_s t) \sin^2 \theta - \sin 2\theta (a \sin \phi + b \cos \phi)\}, \\ P_{A_\times}(\theta, r) = \frac{1}{r} \sin \theta (a \cos \phi - b \sin \phi). \quad (110)$$

We have included the  $r$  dependence in the angular parts of the amplitudes in order to investigate the dependence. Let us note that the time when the radiation reaches the detector is

$$t_{det} = f_1/v_s, \quad (111)$$

then the geometrical structure of  $P_{A_+}(\theta, r)$  changes because of  $f_1 - v_s t_{det} = 0$ . The choice of coordinates enables us to choose  $f_1$ , this change of structure is then just of coordinate nature and has no physical meaning.

In the following figures, we will observe the effect of time dependence of the  $A_+$  amplitude. The angular shape of  $P_{A_+}(\theta, t)$  of the shock wave at start  $t = 0$  is depicted in Fig. 4. The angular dependence has a symmetric shape of toroid with the center at  $z = 0$  ( $\theta = \phi = 0$ ). The surfaces inside the toroid represent angular structure for larger  $r$  and we observe that the magnitude of the toroid becomes smaller, as expected, as  $1/r$ .

At the time shortly before the detector  $t < t_{det}$ , the angular dependence is smaller in Fig. 5 than the one at  $t = 0$  in the previous Fig. 4 but the toroidal geometry remains. The graphs were made for values  $a = b = 10^{-6} \text{m}$ ,  $R_t = 15.144 \text{ kg/m}^3$  for Carbon,  $I_L = 5 \times 10^{26} \text{ W/m}^2$  and  $v_s = 7.21 \times 10^6 \text{ m/s}$ . Then the time when radiation reaches detector is  $t_{det} = 1.387 \mu\text{s}$  and the amplitude  $A_{A_+} = 1.952 \times 10^{-38}$  and  $A_{A_\times} = 3.90 \times 10^{-38}$ .

At the moment  $t_{det}$  when the radiation reaches the detector, one term in the angular dependence vanishes and the geometry of the angular dependence changes. In Fig. 6, we can see the structure of cloverleaf, the four leaves in four sectors which is centered around  $z = 0$ . The surfaces for smaller  $r$  can be seen inside the cloverleaf. We observe that the amplitude of the angular dependence is much smaller than the two previously pictured. Even though the occurrence of this structure is just of coordinate nature, it is interesting to present it in the paper.

The amplitude for polarization mode  $\times$  is pictured in Fig. 7. Moreover, the spherical surface is pictured in the region where  $\phi$  has negative values and  $\theta$  has positive values in radians. It starts at  $z = 0$ , the sphere or bulb grows from that point. The shape stays the same for all times of the experiment duration. The measures are much smaller than the one at images for the  $+$  amplitude, they become comparable at the detector distance.

Interestingly, we investigate the orientation of the both amplitudes toward each other in one figure, see the Fig. 8. The second amplitude is rather small comparable to the toroid which is reduced to a cone in the image. It depicts the center cone of the toroid and the orientation of the  $P_{A_\times}(\theta, r)$  which is present in the part of toroid left out in Fig. 4 for  $r = 1.8 \text{ m}$ . The amplitude becomes comparable at the detector, which is pictured in the second image.

The difference in the time dependency of the two independent polarization modes might be very important for the experimental detection, because it would be possible to distinguish the two modes of polarization. The one mode  $A_+$  would be changing and getting smaller during

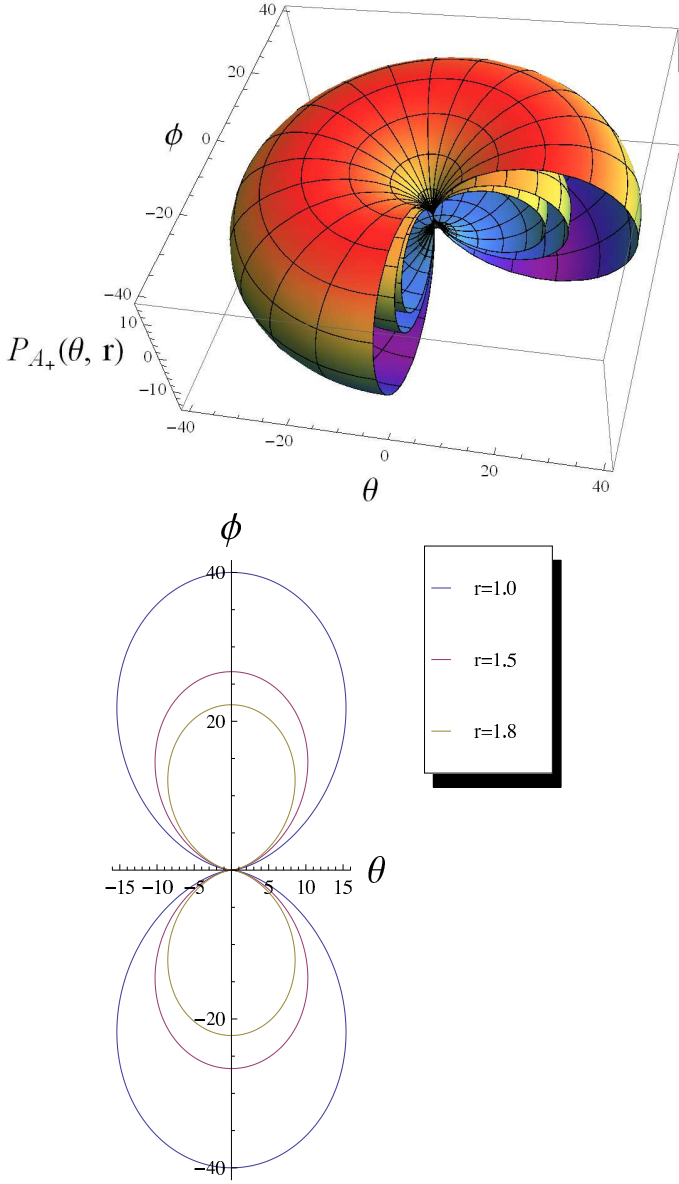


FIG. 4. (Color online) The angular part of amplitude  $P_{A_+}(\theta, r)$  (110) pictured in dependence on  $\theta$  and additional  $\phi$  angle in radians at the time  $t = 0$  in 3D and 2D figures. The amplitude has a shape of toroid with symmetry around axes  $z = 0$ . The dependence on  $1/r$  is depicted in smaller surfaces in the figure, the biggest surface is  $r = 1$  m, then  $r = 1.5$  m and  $1.8$  m. The surface is getting smaller as  $r \rightarrow 10$  m (at the distance of the detector) and approaches 0 as  $r \rightarrow \infty$ . The toroid was cut on purpose to see the inner surfaces of lower  $r$ . The polar 2D diagram was plotted for fixed angle  $\phi = \pi/2$ .

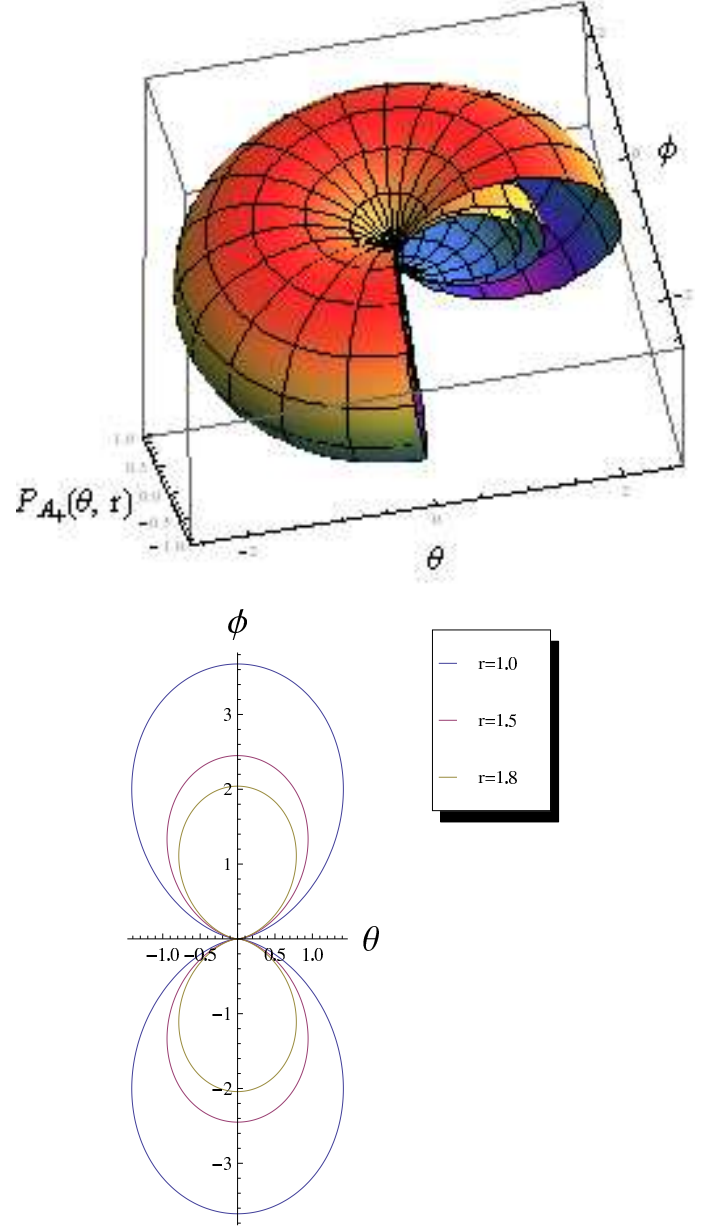


FIG. 5. (Color online) The angular part of amplitude  $P_{A_+}(\theta, r)$  (110) pictured in dependence on  $\theta$  and additional  $\phi$  angle in radians at the time  $t = 1.3 \mu\text{s}$  in 3D and 2D figures. The dependence on  $1/r$  is depicted in smaller surfaces in the figure, the biggest surface is  $r = 1$  m, then  $r = 1.5$  m and  $1.8$  m. The surface is getting smaller as  $r \rightarrow 10$  m (at the distance of the detector) and approaches 0 as  $r \rightarrow \infty$ . The magnitude of the diagram is significantly smaller than in the Fig. 4.

### C. The radiative characteristics for generated gravitational waves

the time of the experiment compared to the other, constant one  $A_\times$ , which could be measurable in principle.

The energy and momentum carried by the GWs at large distances from the source (at position of the detec-

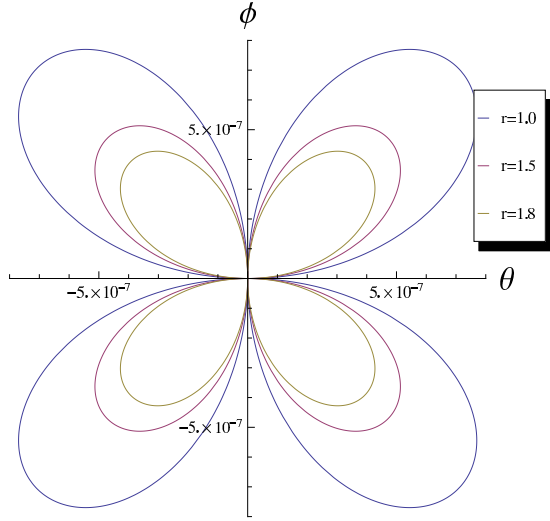
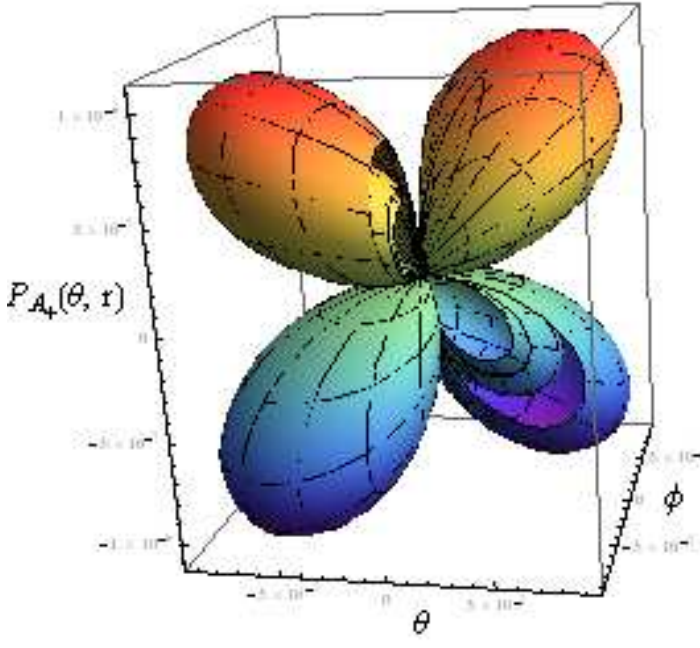


FIG. 6. (Color online) The angular part of amplitude  $P_{A_+}(\theta, r)$  (110) pictured in dependence on  $\theta$  and additional  $\phi$  angle in radians at the detector in 3D and 2D figures. The geometry of toroid changed into cloverleaf geometry with symmetry around  $z = 0$ . The magnitude of the angular part of amplitude is much smaller than previous ones. The polar 2D diagram was plotted for fixed angle  $\phi = \pi/2$ .

tor) is described by the effective tensor

$$t_{\mu\nu}^{GW} = \frac{c^4}{32\pi G} \langle \partial_\mu h_{\alpha\beta} \partial_\nu h^{\alpha\beta} \rangle, \quad (112)$$

where the brackets mean averaging over frequencies in one period of time and the tensor (112) satisfies the energy conservation  $\partial^\mu t_{\mu\nu} = 0$ , [34, 35].

In particular, the invariant energy density can be ex-

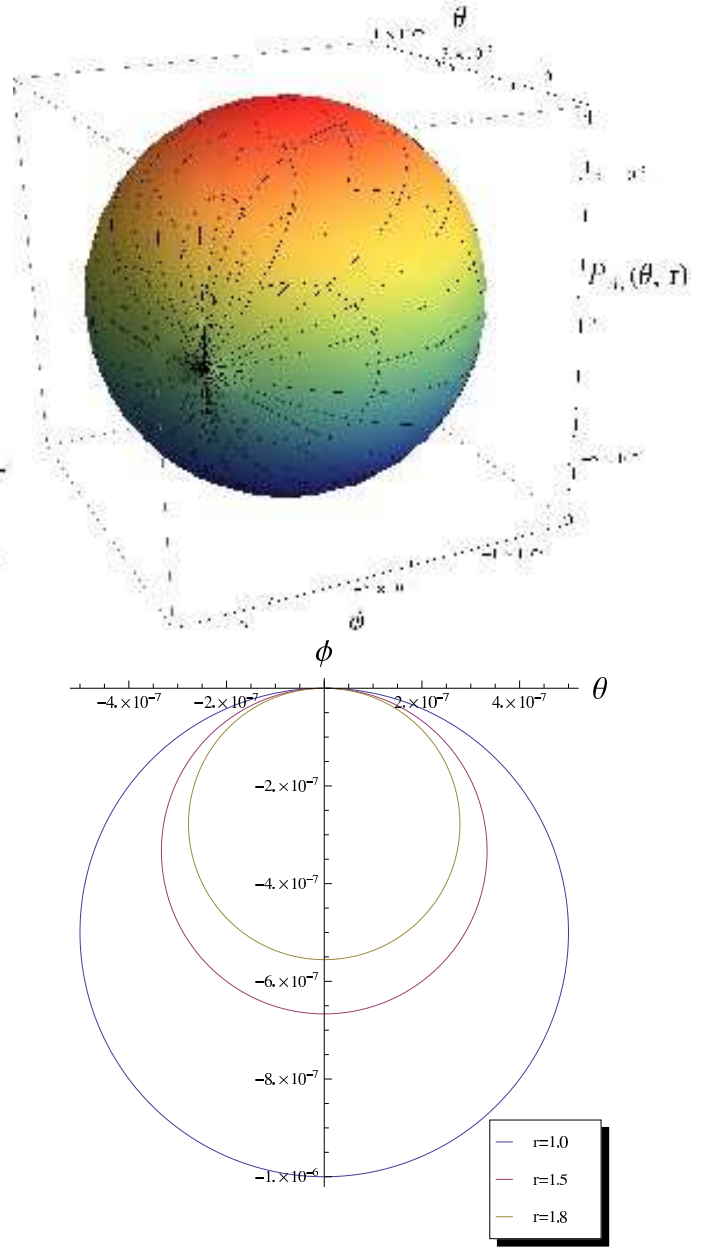


FIG. 7. (Color online) The angular part of amplitude  $P_{A_\times}(\theta, r)$  (110) pictured in dependence on  $\theta$  and additional  $\phi$  angle in radians at any time. The surface is getting smaller as  $r \rightarrow 10$  m (the distance of the detector) and approaches 0 as  $r \rightarrow \infty$ . The dependence on  $1/r$  is depicted in smaller surfaces in the polar figure, the biggest surface is  $r = 1$  m, then  $r = 1.5$  m and 1.8 m where we have chosen  $\phi = \pi/2$ .

pressed as

$$t_{GW}^{00} = \frac{c^4}{32\pi G} \langle \dot{h}_{ij}^{TT} \dot{h}_{ij}^{TT} \rangle = \frac{c^4}{32\pi G} \langle \dot{A}_+^2 + \dot{A}_\times^2 \rangle. \quad (113)$$

In our case, the  $A_\times$  amplitude is time-independent for our models, therefore just the  $A_+$  contributes to the

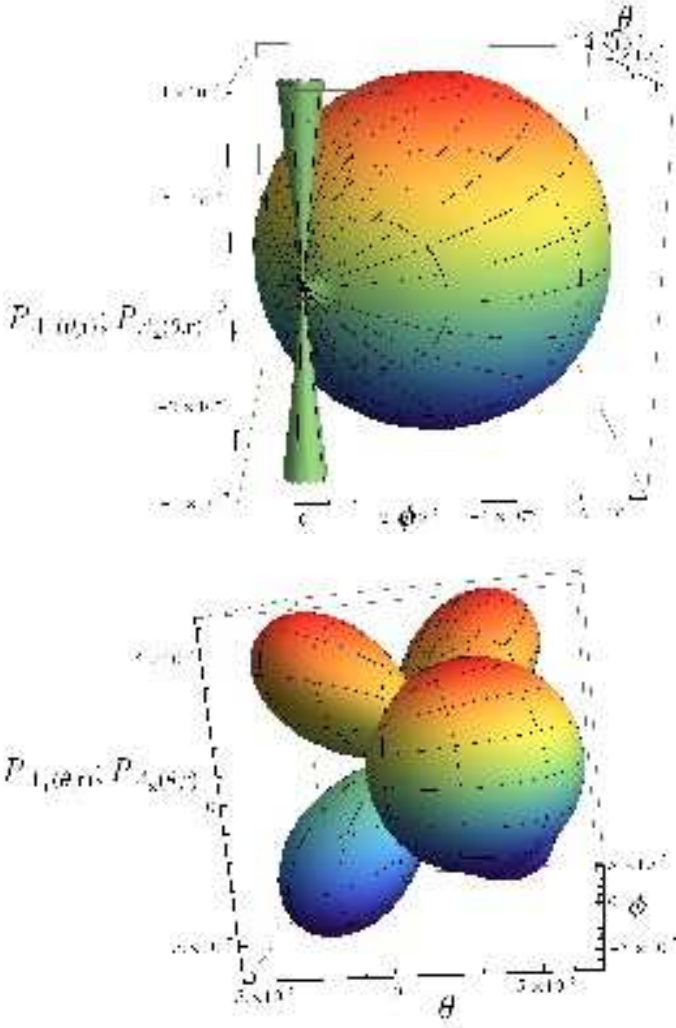


FIG. 8. (Color online) The angular part of amplitude  $P_{A_x}(\theta, r)$  (110) and  $P_{A_x}(\theta, r)$  pictured in dependence on  $\theta$  and additional  $\phi$  angle in radians together in one figure for comparison. The second amplitude is rather small compared to the toroid which is reduced to a cone in the image. It depicts the center cone of the toroid and the orientation of the  $P_{A_x}(\theta, r)$  which is present in the part of toroid left out in Fig. 4. The amplitude becomes comparable at the detector, which is pictured in the second image. The pictures are for  $r = 1.8$  m.

effective tensor,

$$t_{00}^{GW} = \frac{c^4}{32\pi G} \langle \dot{A}_+^2 \rangle = \frac{9}{8\pi} \frac{G}{r^2 c^4} S^2 \rho_0^2 v_s^6 \sin^4 \theta, \quad (114)$$

which functionally depends on  $r$  and  $\theta$  angle. The energy goes to zero as  $r$  approaches infinity. The energy spectrum is then trivial  $\frac{dE}{dA} = \frac{c^3}{16\pi G} \int_0^\tau dt \dot{A}_+^2 = \frac{c^3}{16\pi G} \dot{A}_+^2 \tau$  where  $dA = r^2 d\Omega$  is surface element and  $\tau$  is duration of pulse.

The radiative characteristic represents amount of energy going through various directions in the case of large

distances  $r$  for quadrupole radiation. We can obtain it by using (112) and rewrite as

$$-t_{0r}^{GW} \equiv S = \frac{c^3}{72G\pi r^2} \langle \ddot{I}_{ij} \ddot{I}_{ij} - 2\ddot{I}_{is} \ddot{I}_{sj} n_i n_j + \frac{1}{2} \ddot{I}_{ij} \ddot{I}_{rs} n_i n_j n_r n_s \rangle. \quad (115)$$

The luminosity  $\mathcal{L}_{GW}$  defined in the beginning as (37) is connected to  $t_{\mu\nu}^{GW}$

$$-\frac{dE}{dt} = \mathcal{L}_{GW} = \int t_{0r}^{GW} r^2 \sin\theta d\theta d\phi, \quad (116)$$

which can be found by integration over a sphere with diameter  $r$ .

We will express the equation (115) for the orientation of wave vector into  $x, y$  and  $z$  directions.

The expression (115) for the orientation of the wave vector to  $x$  direction reads,

$$\mathcal{S}_{n_x} = \frac{c^3}{72G\pi r^2} \left[ -\frac{1}{2} (\ddot{I}_{xx})^2 + (\ddot{I}_{yy})^2 + (\ddot{I}_{zz})^2 + 2(\ddot{I}_{yz})^2 \right], \quad (117)$$

for the orientation of the wave vector to  $y$  direction,

$$\mathcal{S}_{n_y} = \frac{c^3}{72G\pi r^2} \left[ (\ddot{I}_{xx})^2 - \frac{1}{2} (\ddot{I}_{yy})^2 + (\ddot{I}_{zz})^2 + 2(\ddot{I}_{xz})^2 \right], \quad (118)$$

and finally, the orientation of the wave vector to  $z$  direction,

$$\mathcal{S}_{n_z} = \frac{c^3}{72G\pi r^2} \left[ (\ddot{I}_{xx})^2 + (\ddot{I}_{yy})^2 - \frac{1}{2} (\ddot{I}_{zz})^2 + 2(\ddot{I}_{xy})^2 \right]. \quad (119)$$

We can evaluate (115) for the general wave vector (102) as

$$\begin{aligned} \mathcal{S}_n = & \frac{c^3}{72G\pi r^2} [(\ddot{I}_{xx})^2 (1 - 2\sin^2\theta \sin^2\phi) \\ & + (\ddot{I}_{yy})^2 (1 - 2\sin^2\theta \cos^2\phi) + (\ddot{I}_{zz})^2 (1 - 2\cos^2\theta) \\ & + \frac{1}{2} (\ddot{I}_{xx} \sin^2\theta \sin^2\phi + \ddot{I}_{yy} \sin^2\theta \cos^2\phi + \ddot{I}_{zz} \cos^2\theta)^2], \end{aligned} \quad (120)$$

where the expression simplifies since  $\ddot{I}_{xy} = \ddot{I}_{xz} = \ddot{I}_{yz} = 0$ .

Now, we are able to substitute the ansatz for the  $z_s$  into (117), (118), (119) and (120). Then the expressions for the wave vector in directions  $n = x, y, z$  read,

$$\begin{aligned} \mathcal{S}_{n_x} &= \frac{c^3}{4G\pi r^2} S^2 \rho_0^2 v_s^6, \\ \mathcal{S}_{n_y} &= \frac{c^3}{4G\pi r^2} S^2 \rho_0^2 v_s^6, \\ \mathcal{S}_{n_z} &= 0, \end{aligned} \quad (121)$$

and the expression for the general wave vector (102) results in

$$\mathcal{S}_n = \frac{S^2 c^3 \rho_0^2 v_s^6}{36G\pi r^2} [12 - 4(\sin^2 \theta + 2 \cos^2 \theta) + (2 \cos^2 \theta - \sin^2 \theta)^2]. \quad (122)$$

The radiative characteristics (122) depends only on the  $\theta$  angle which is a consequence of the axis symmetry of the problem. It behaves as  $1/r^2$  as  $r \rightarrow \infty$  contrary to  $1/r$  decay of amplitudes. To visualize the radiative characteristic, it is useful to separate the angular part from its amplitude as

$$\mathcal{S}_n = \frac{S^2 c^3 \rho_0^2 v_s^6}{36G\pi} P_{S_n}(\theta, r) \quad (123)$$

where the angular dependence is given as

$$P_{S_n}(\theta, r) = \frac{1}{r^2} [12 - 4(\sin^2 \theta + 2 \cos^2 \theta) + (2 \cos^2 \theta - \sin^2 \theta)^2]. \quad (124)$$

The radiation structure is pictured in Fig. 9 where the structure of the surface corresponds roughly to the non-relativistic radiation structure of accelerated particle [34]. The shock wave model is used in non-relativistic calculations therefore the result agrees with this fact. The extreme values of the function  $P_{S_n}(\theta, r)$  of the angle  $\theta$  correspond to the values of  $\theta$  where it is valid  $\sin 2\theta = 0$  or  $2/3 = \cos^2 \theta + \cos 2\theta$ .

The amplitude  $A_{S_n} = \frac{S^2 c^3 \rho_0^2 v_s^6}{36G\pi}$  (123) has a specific value  $A_{S_n} = 1.49 \times 10^{51}$  for  $a = b = 10^{-6}$  m,  $R_t = 15.144$  kg/m<sup>3</sup> for Carbon,  $I_L = 5 \times 10^{26}$  W/m<sup>2</sup> and  $v_s = 7.21 \times 10^6$  m/s. The polar dependence on  $\theta$ ,  $\phi$  and  $r$  is plotted in Fig. 10 and the dependence on  $\theta$  and  $r$  is plotted in Fig. 11.

This directional characteristic tells us, in fact, where to expect the gravitational radiation and where not, therefore it is one of the main results of the paper. The experimental set up and positions of the detectors should be adjusted to the directional characteristic to make the experiment the most effective.

#### D. The angular momentum

The gravitational waves carry away energy and angular momentum, the angular momentum carried away per unit time by the gravitational waves is given by

$$\left( \frac{dJ^i}{dt} \right)_{quad} = \frac{2G}{5c^5} \epsilon^{ikl} \ddot{I}_{ka} \ddot{I}_{la}, \quad (125)$$

where the derivatives of the quadrupole moment are evaluated at the retarded time  $t - r/c$ , [4, 34].

When substituting the derivatives quadrupole moment (A 3), we will obtain that

$$\left( \frac{dJ^i}{dt} \right)_{quad} = 0 \longrightarrow J^i = \text{const.} \quad (126)$$

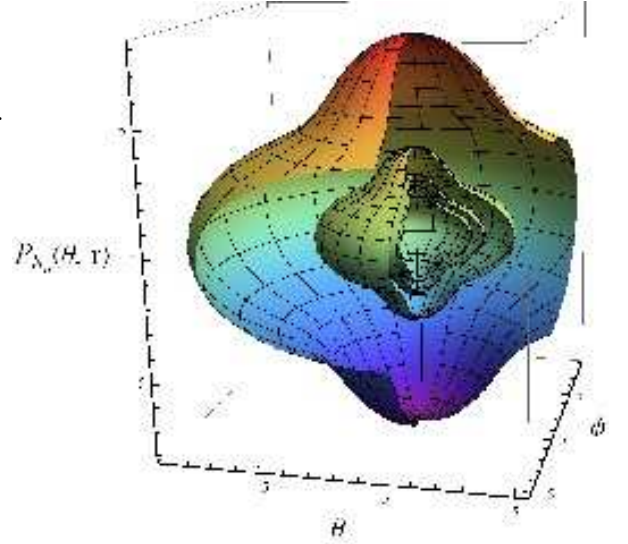


FIG. 9. (Color online) The radiation characteristics  $\mathcal{S}_n$  (122) pictured in dependence on  $\theta$  angle and rotated additionally around  $\phi$  angle in radians. We have plotted just the angular dependence  $P_{S_n}(\theta, r)$  (124),  $\mathcal{S}_n = A_{S_n} P_{S_n}(\theta, r)$ , (123). The dependence on  $1/r^2$  is depicted in smaller surfaces in the figure, the biggest surface is  $r = 1$  m, then  $r = 1.5$  m,  $1.8$  m and  $r = 2$  m. The surface is getting smaller as  $r \rightarrow 10$  m (the distance of the detector), while  $r \rightarrow \infty$  the surface approaches 0. The structure of surfaces is symmetric around the axes  $z = 0$ . The structure of the surface corresponds to the non-relativistic radiation structure [34].

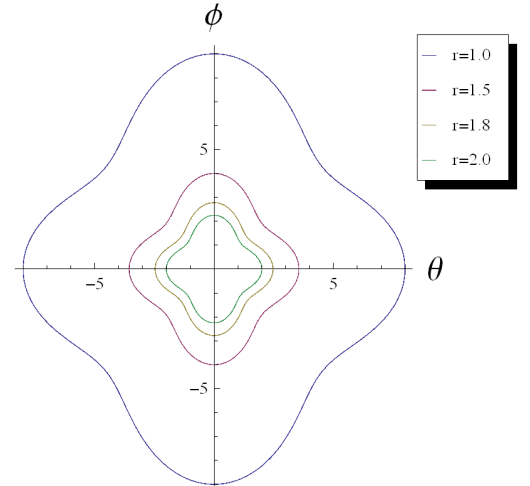


FIG. 10. (Color online) The radiation characteristics  $\mathcal{S}_n$  (122) pictured in polar coordinates  $\theta$  and  $\phi$  in radians. We have plotted just the angular dependence  $P_{S_n}(\theta, r)$  (124). The picture represents the cuts at  $r = 1; 1.5; 1.8; 2$  m.

The angular momentum of the radiation in the shock wave model stays constant in time. Which is due to the linear movement of shock wave. The situation will be different in case of rotating stick or double-star.

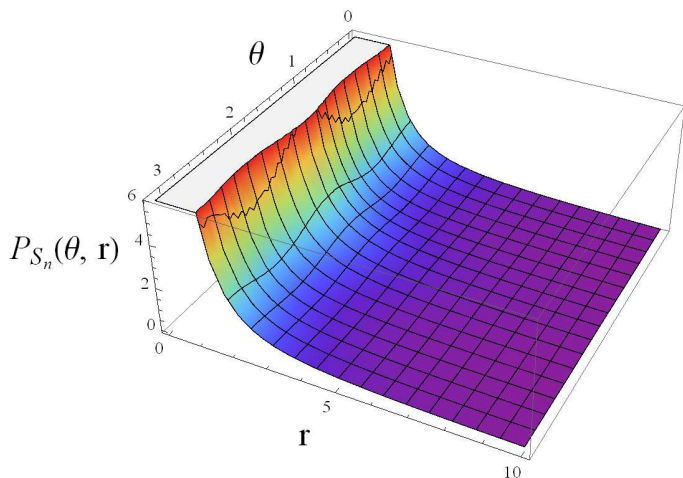


FIG. 11. (Color online) The radiation characteristics  $\mathcal{S}_n$  (122) pictured in polar coordinates  $\theta$  in radians and  $r$  in meters. Just the angular dependence is plotted  $P_{\mathcal{S}_n}(\theta, r)$  (124). The radiation tends to small values for  $r = 10$  m and vanishes at infinity.

## V. THE BEHAVIOR OF TEST PARTICLES IN THE PRESENCE OF A GRAVITATIONAL WAVE

In this section we will introduce the notion of the influence of the gravitational field of gravitational wave on two close particles and define their equation of motion, called the equation of deviation, in local reference frame. Then we will be able to analyse the distance of two particles for our models.

Let assume two neighbouring particles A and B where we will examine the movement of the particles from point of view of particle A. We will use proper reference frame of A, with origin  $x^j = 0$  which is attached to world line, the coordinate time is equal to proper time of A ( $x^0 = \tau$  on world line  $x^j = 0$ ) and with orthonormal spatial axes attached to gyroscopes carried by A (non-rotating frame). This coordinate system is a local Lorentz frame along all the world line of A, connected to the local inertial frame of the particle A:

$$g_{\mu\nu} = -dx^0{}^2 + \delta_{jk}dx^j dx^k + O(|x^j|^2)dx^\alpha dx^\beta. \quad (127)$$

When the gravitational wave passes, it produces an oscillating curvature tensor which twists the distance vector from particle A to particle B. A is at the origin of its own proper reference frame, then the separation vector  $n^j = x_B^j - x_A^j = x_B^j$  because  $x_A^j = 0$ .

The equation of deviation is the following

$$\frac{d^2 x_B^j}{dt^2} = -R_{j0k0} x_B^k = \frac{1}{2} \frac{\partial^2 h_{jk}^{TT}}{\partial t^2} x_B^k, \quad (128)$$

which describes the relative acceleration of two particles originally moving along two parallel trajectories in proper

detector frame. We have used the fact that to first order in  $h_{ij}^{TT}$ ,  $t = \tau + O(h)$ .

The equation (128) can be integrated if we assume that the particles are at rest relative to each other before the wave arrives (when  $h_{ij}=0$  then  $x_B^j = x_{B(0)}^j$ ).

The equation of motion yields

$$x_B^j(\tau) = x_{B(0)}^k \left[ \delta_{jk} + \frac{1}{2} h_{jk}^{TT}(\tau) \right]_{\text{at position of A}} \quad (129)$$

and describes the oscillations of particle B's location measured in the reference frame of particle A.

For the case of a plane wave, there is no oscillation in the direction of the propagation of the wave,  $h_{jk}^{TT} x_{B(0)}^k = 0$ . Our result for the wave vector oriented in the  $z$  direction (83) fully agrees with the property. Then the plane gravitational wave has transversal character similarly to the electromagnetic wave. This property is valid in full gravity theory and therefore the plane wave example is significant one. The position of the second particle B can be affected by the wave just in transversal directions to the wave propagation direction.

### A. The predictions for the detector

The equation of deviation (128) is valid as long as  $|x_B|$  is much smaller than typical scale over which the gravitational field changes substantially. For GW, the length scale is the reduced wavelength  $\lambda$ . Then if the detector has characteristic linear size  $L$ , we can discuss its interaction with GW using the equation of deviation only if

$$L \ll \lambda, \quad (130)$$

where  $\lambda = \lambda/2\pi$  is reduced wave length of the gravitational wave.

If the condition (130) is not satisfied the full relativity approach would be necessary. For example, the bar detectors and ground based interferometers satisfy (in the first approximation) this condition but LISA does not.

According to (130), we can estimate the linear size  $L$  of the possible detector as

$$L \ll 4.7746 \times 10^{-2} \text{ m}, \quad (131)$$

which might serve as useful estimation for validity of the future experiment and the detector. We have used the numerical values mentioned in (III B).

### B. Movement of particles

First, we will investigate the effect of the linearly polarized gravitational wave on test particles in the mode + for the wave vector in  $x$  direction (IV A 2) because the case for  $z$  direction is trivial. Since the propagation of the laser occurs in the  $z$  direction and the wave vector is

oriented in the  $x$  coordinate, the movement will happen in the  $(z, y)$  plane. We assume that the test particles are set on a circle of radius  $r = a$  at time  $\tau = 0$ . In the center of the circle is the reference particle A, which is at rest in the proper reference frame. The position of the particle in any time is defined by (129). We will denote the coordinate in the reference frame as  $\tilde{x}$ ,  $\tilde{y}$  and  $\tilde{z}$ , then we will get for near particle in time  $\tau$  for  $A_\times = 0$ ,

$$\begin{aligned}\tilde{z}_B(\tau) &= \left[ 1 + \frac{1}{2} h_{zz}^{TT}(\tau)|_{\tilde{x}_A^j=0} \right] \tilde{z}_{B(0)}, \\ \tilde{y}_B(\tau) &= \left[ 1 - \frac{1}{2} h_{zz}^{TT}(\tau)|_{\tilde{x}_A^j=0} \right] \tilde{y}_{B(0)},\end{aligned}\quad (132)$$

where we have used  $h_{zz}^{TT} = -h_{yy}^{TT}$ ,  $z_{B(0)} = a \cos \phi$  and  $y_{B(0)} = a \sin \phi$  which are coordinates in time  $\tau = 0$  when the particles were distributed along the circle of radius  $a$ . In the further text, we assume all  $h_{ij}^{TT}|_{\tilde{x}_A^j=0}$  (i.e. are evaluated at  $\tilde{x}_A^j = 0$ ) and we will not write it explicitly.

The expression  $\cos^2 \phi + \sin^2 \phi = 1$  then leads to

$$\left\{ \frac{\tilde{z}_B(\tau)}{a[1 + \frac{1}{2} h_{zz}(\tau)]} \right\}^2 + \left\{ \frac{\tilde{y}_B(\tau)}{a[1 - \frac{1}{2} h_{zz}(\tau)]} \right\}^2 = 1, \quad (133)$$

which is equation of ellipse with semi-minor axes  $a[1 \pm \frac{1}{2} h_{zz}(\tau)]$ . The reference frame has origin at  $\tilde{x} = \tilde{y} = \tilde{z} = 0$  and in the coordinates of TT gauge  $x = y = 0$  and  $z = f_1$  and  $t = \tau + O(h)$ . For convenience, we will shift the origin of the coordinates to  $z = f_1$ , then the coordinates of TT will be  $x = y = 0$  and  $z = 0$  and  $t = \tau + O(h)$ .

Recall that we take real part of  $h_{zz}^{TT}$  (12),

$$\begin{aligned}h_{zz}(\tau) &= \text{Re} \{ A_+ e^{-i\omega\tau} \} \\ &= (\text{Re} A_+) \cos \omega\tau - (\text{Im} A_+) \sin \omega\tau,\end{aligned}\quad (134)$$

where we observe that  $\text{Im} A_+ = 0$  then  $h_{zz}(\tau) = A_+ \cos \omega\tau$ . Without losing any information, we perform a phase shift,  $+\pi/2$ , and get  $h_{zz}(\tau) = A_+ \sin \omega\tau$ . When  $\tau = 0$  then  $h_{zz} = h_{zz}(\tau) = 0$ . Without the shift in  $TT$  coordinates the component  $h_{zz} = f(f_1)$  will be non-zero.

The semi-minor axes are

$$a[1 \pm A \sin \omega\tau], \quad (135)$$

where  $A = \frac{1}{2} A_+$  and

$$A \equiv A|_{\tilde{x}_A^j=0} = \frac{3}{r} \frac{G}{c^4} S \rho_0 v_s^2 (-v_s \tau), \quad (136)$$

the explicit form of  $\frac{1}{2} h_{zz}^{TT}(\tau)|_{\tilde{x}_A^j=0}$  then is

$$\frac{1}{2} h_{zz}^{TT}(\tau)|_{\tilde{x}_A^j=0} = \frac{3}{r} \frac{G}{c^4} S \rho_0 v_s^2 (-v_s \omega\tau) \sin \omega\tau. \quad (137)$$

The negativity of the amplitude just means that the change will happen in the transversal direction to the positive one.

To see the behavior of test particles, we use (132) and (137). In our specific case, the ellipse will be changing its shape due to the time dependency of the amplitude  $A_+$ , see Fig. 12.

The initial position of test particles on circle at  $\tau = 0$ , (Fig. 12(a)), is gradually changing into ellipse (Fig. 12(b)) due to the influence of the wave, into the direction of  $\tilde{y}_B$ , then it changes to circle (Fig. 12(c)), then ellipse prolonged in  $\tilde{z}_B$  (Fig. 12(d)) and then back to circle (Fig. 12(a)).

In Fig. 12(b) and 12(d), the time dependence of the amplitude is demonstrated explicitly. In Fig. 12(b) we observe the changing of the ellipse to a sharper profile as the time grows,  $\tau = \pi/2/\omega; 5\pi/2/\omega; 9\pi/2/\omega$ , etc., in Fig. 12(d) the ellipse gets sharper profile in the transversal direction for times  $\tau = 3\pi/2/\omega; 7\pi/2/\omega; 11\pi/2/\omega$ , etc.

For demonstrational purposes, we have used  $\frac{1}{2} h_{zz}^{TT}(\tau)|_{\tilde{x}_A^j=0} = -0.45 \omega\tau \sin \omega\tau$  to make the effect of time dependent amplitude visible. The real value is very small and difficult to plot. For specific value,  $a = 10^{-6} \text{m}$ ,  $R_t = 15.144 \text{ kg/m}^3$  for Carbon,  $I_L = 5 \times 10^{26} \text{ W/m}^2$ ,  $v_s = 7.21 \times 10^6 \text{ m/s}$  and  $\omega = 2\pi c/\lambda = 6.26 \times 10^{12}$  where  $\lambda = 300 \mu\text{m}$ . Then we get the amplitude  $A = -2.81418 \times 10^{-32} \tau$ .

In the mode  $\times$  we will get also deformation of a circle with the only non-zero component  $h_{zy}^{TT}$ . The equation (129) for  $A_+ = 0$  gives

$$\begin{aligned}\tilde{z}_B(\tau) &= \frac{1}{2} h_{zy}^{TT}(\tau)|_{x_A^j=0} \tilde{y}_{B(0)} + \tilde{z}_{B(0)}, \\ \tilde{y}_B(\tau) &= \tilde{y}_{B(0)} + \frac{1}{2} h_{yz}^{TT}(\tau)|_{x_A^j=0} \tilde{z}_{B(0)},\end{aligned}\quad (138)$$

where the pictures from Fig. 12 will be rotated for  $45^\circ$ . Contrary to electromagnetism, where the two orthogonal polarizations are transferable by rotation of  $90^\circ$ . Again, without losing any information, we perform a phase shift,  $\pi/2$ , and get  $h_{yz}(\tau) = A_\times \sin \omega\tau$ , then for  $\tau = 0$  we get  $h_{yz} = 0$ , the explicit form of  $h_{yz}$  then become

$$\frac{1}{2} h_{yz}^{TT}(\tau)|_{\tilde{x}_A^j=0} = -\frac{3}{r} \frac{G}{c^4} S \rho_0 v_s^2 \sin \omega\tau. \quad (139)$$

The negative sign of the amplitude  $A_\times$  just changes the orientation of ellipse in the transversal direction, therefore we observe that the standard orientation of ellipses [4] is rotated around the  $\tilde{z}_B$  axes. The component  $h_{yz}^{TT}$  has constant amplitude therefore the ellipses do not change shape when time grows. In the Fig. 13, the diagrams are plotted to demonstrate the movement of test particles in  $e_\times$  polarization. We have used  $\frac{1}{2} h_{yz}^{TT}(\tau)|_{\tilde{x}_A^j=0} = -5 \sin \omega\tau$  for demonstration purposes, because when we substitute the numbers into it, we get very small number and it is difficult to plot it. For values  $a = b = 10^{-6} \text{m}$ ,  $R_t = 15.144 \text{ kg/m}^3$  for Carbon,  $I_L = 15 \times 10^{26} \text{ W/m}^2$  and  $v_s = 7.21 \times 10^6 \text{ m/s}$  then amplitude  $\frac{1}{2} h_{yz}^{TT}(\tau)|_{\tilde{x}_A^j=0} = -1.95218 \times 10^{-45} \sin \omega\tau$ . The amplitude of the  $A_\times$  is significantly smaller than the amplitude  $A_+$  therefore we observe that the two polarizations might be very easy to distinguish in the experiment.

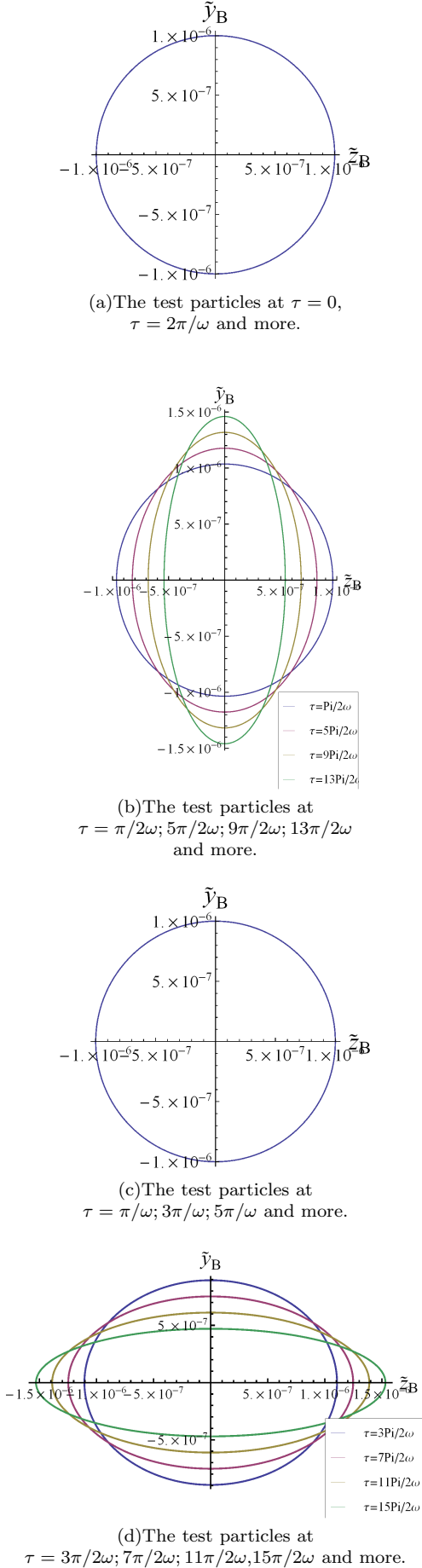


FIG. 12. (Color online) The diagrams depict the position of test particles as function of time under influence of GW wave with + polarization.

The another direction of the wave vector is in the  $y$  direction. The diagrams will look similar, the plane would be  $(x, z)$  and the diagrams Fig. 13(b) and 13(d) for  $\times$  polarization will be rotated for  $45^\circ$  because the amplitude  $A_\times$  has opposite sign to the one for  $x$  direction discussed in detail in this section.

If investigated in circular polarization we would observe rotation of ellipses in right or left directions. The diagrams will not change in rotation  $\pm\pi$ , therefore we deduce the helicity of gravitational waves is  $h = \pm 2$ . We can obtain this result rigorously by performing a rotation by angle  $\theta$  where in  $h_{ij}$  just  $e_{+ij}$  and  $e_{\times ij}$  transform,  $\mathbf{e}'_1 = \mathbf{e}_1 \cos \theta + \mathbf{e}_2 \sin \theta$ ,  $\mathbf{e}'_2 = -\mathbf{e}_1 \sin \theta + \mathbf{e}_2 \cos \theta$ ,  $\mathbf{e}'_{+ij} = \mathbf{e}_{+ij} \cos 2\theta + \mathbf{e}_{\times ij} \sin 2\theta$ ,  $\mathbf{e}'_{\times ij} = -\mathbf{e}_{+ij} \sin 2\theta + \mathbf{e}_{\times ij} \cos 2\theta$ , therefore  $\mathbf{e}'_{+ij} = \mathbf{e}_{+ij}$ ,  $\mathbf{e}'_{\times ij} = \mathbf{e}_{\times ij}$  for  $\theta = \pm\pi$ . For combination  $h_{zz} \mp ih_{zy}$  the relation  $\psi' = e^{ih\theta}\psi$  where  $\psi$  is any field in case of plane waves with zero mass and  $\theta$  is the spacetime rotation angle in planes transversal to the wave propagation direction, [4, 34].

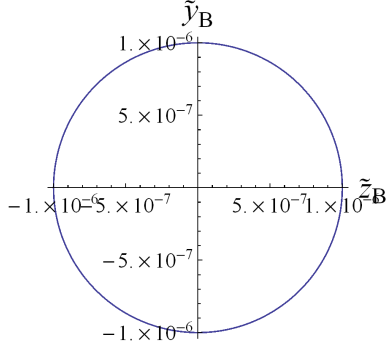
In this section, we have investigated behavior of test particles in the presence of GW with two modes of polarization. The main result is that the time dependent amplitude of polarization + influences the circle of particles to change the shape to ellipse and as time is passing the ellipse shape becomes sharper. The  $\times$  polarization of the GW influences the circle of test particles to change the shape to ellipse shifted by  $45^\circ$  and the shape stays constant in time. This might serve as a measurable quality in the future experiments.

## VI. CONCLUSION

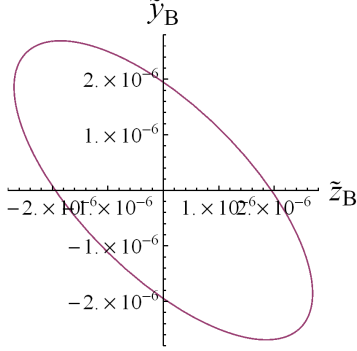
We have investigated models for the generation of gravitational waves in three different experiments in laboratory conditions. The models for experiments are based on high power laser-matter interaction. The paper is divided into two separate papers. In this first paper, we concentrate on the shock wave model. The next paper (part II) will concentrate on the ablation and piston models.

We have verified that linear gravity can be used for the shock wave model, calculated and analyzed the perturbation tensor  $h_{ij}^{TT}$  and the luminosity of gravitational radiation  $\mathcal{L}_{GW}$  in low velocity approximation far away from the source. The results presented in [23, 24] were generalized to include the dependence on the laser wavelength and material of the foil. The calculations are presented in detail and estimations for real experimental values are included.

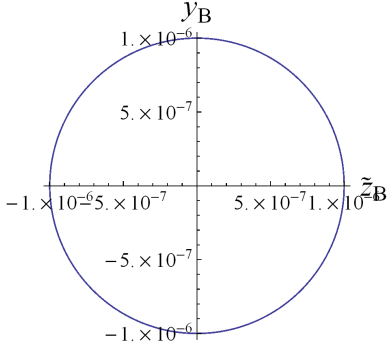
We have also investigated the two independent polarization modes of the gravitational radiation in the shock wave model. The amplitudes of the radiation were derived in the three main directions of wave propagation,  $x, y, z$ . The radiation vanishes in the direction of motion in the  $z$  direction. The radiation is non-vanishing in other directions such as  $x$  and  $y$  directions, the amplitude for mode + of the polarization occurs as time



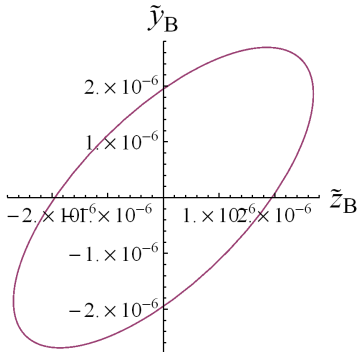
(a) The test particles at  $\tau = 0$ ,  
 $\tau = 2\pi/\omega$  and more.



(b) The test particles at  
 $\tau = \pi/2\omega; 5\pi/2\omega; 9\pi/2\omega; 13\pi/2\omega$  and  
more.



(c) The test particles at  
 $\tau = \pi/\omega; 3\pi/\omega; 5\pi/\omega$  and more.



(d) The test particles at  
 $\tau = 3\pi/2\omega; 7\pi/2\omega; 11\pi/2\omega; 15\pi/2\omega$   
and more.

FIG. 13. (Color online) The diagrams depict the position of test particles as function of time under influence of GW wave with  $\times$  polarization.

dependent and the other amplitude for mode  $\times$  is time-independent. This is an important result which might be measured in the real experiment. Furthermore, the radiative characteristics in the general wave direction given by angles  $\theta$  and  $\phi$  was investigated. The obtained directional structure of radiation is dependent on the two angles. Again the amplitude for mode  $+$  is time dependent and for mode  $\times$  is time-independent in the general case. The result might be used for positioning of detectors in real experiments.

Then the influence of gravitational waves was analyzed on test particles using the geodesics equation. The difference in amplitudes of the two modes of polarization was demonstrated and visualized in greater detail.

The proposed experiments can be performed at Petawatt laser facilities such as ELI (Czech Republic) [27], APOLLON (France) [37], APRI-GIST (South Korea) [38], OMEGA-EP (USA) [39] or FIREX (Japan) [40].

Therefore the remaining problem is the detection of the gravitational waves which have the amplitude of the metric perturbation around  $10^{-40}$  which is almost 20 orders lower than the detected radiation from space [2]. The frequencies are in the GHz – THz range therefore the gravitational waves can't be detected by any of the known detectors like interferometers or the Weber resonators. The suggested Li-Baker detector is one candidate for the detection of high frequency waves (10 GHz) because it uses a different technology. The lowest detectable perturbation range is around  $10^{-37}$  which is almost suitable for detection in shock and ablation models. The frequencies of piston model (THz) are still higher than the frequency range of Li-Baker detector. The Li-Baker detector is still in the first stage of development. Further improvement for the future to work in higher frequency range and in even lower sensitivity level might enable the measurement of the gravitational waves produced by the presented models.

## ACKNOWLEDGMENTS

H. Kadlecová wishes to thank Tomáš Pecháček for many valuable discussions and time, and Otakar Svíttek for his valuable comments. The work was supported by the ELI project No. CZ.02.1.01./0.0/0.0/15-008/0000162.

## Appendix A: Derivatives for the shock wave model

### 1. The derivatives of an ansatz for $z_s$

The derivatives of the function  $z_s(t)$  are

$$\begin{aligned} (z_s^2)' &= 2z_s \dot{z}_s, & (z_s^2)'' &= 2\{(\dot{z}_s)^2 + z_s(z_s)''\}, \\ (z_s^2)''' &= 2\{3\dot{z}_s \ddot{z}_s + z_s(z_s)'''\}, \\ (z_s^3)' &= 3z_s^2 \dot{z}_s, & (z_s^3)'' &= 3z_s\{2(\dot{z}_s)^2 + z_s \ddot{z}_s\}, \\ (z_s^3)''' &= 3\{2(\dot{z}_s)^3 + 6z_s \dot{z}_s \ddot{z}_s + z_s^2(z_s)'''\}. \end{aligned} \quad (\text{A1})$$

and after the ansatz for the  $z_s$  we get

$$\begin{aligned} z_s &= -v_s t + d, & \dot{z}_s &= -v_s, & \ddot{z}_s &= 0, \\ (z_s^2)' &= 2(-v_s t + d)\dot{z}_s, & (z_s^2)'' &= 2v_s^2, & (z_s^2)''' &= 0, \\ (z_s^3)' &= -3v_s(-v_s t + d)^2, & (z_s^3)'' &= 6v_s^2(-v_s t + d), \\ (z_s^3)''' &= -6v_s^3, & (z_s^3)'''' &= 0. \end{aligned} \quad (\text{A2})$$

### 2. The derivatives of mass moment and quadrupole moment with $z_s$ function

For calculation purposes we will present, first, second and third derivatives with respect to time, of the quadrupole moments here. The first derivatives of non-diagonal components are

$$\begin{aligned} \dot{I}_{xy} = \dot{M}_{xy} &= -\frac{3}{4}S^2\rho_0 \dot{z}_s, & \dot{I}_{yz} = \dot{M}_{yz} &= -\frac{3}{4}Sb\rho_0(z_s^2)', \\ \dot{I}_{xz} = \dot{M}_{xz} &= -\frac{3}{4}Sa\rho_0(z_s^2)', \end{aligned} \quad (\text{A3})$$

and the second derivatives are

$$\begin{aligned} \ddot{I}_{xy} = \ddot{M}_{xy} &= -\frac{3}{4}S^2\rho_0 \ddot{z}_s, & \ddot{I}_{yz} = \ddot{M}_{yz} &= -\frac{3}{4}Sb\rho_0(z_s^2)'' , \\ \ddot{I}_{xz} = \ddot{M}_{xz} &= -\frac{3}{4}Sa\rho_0(z_s^2)'' , \end{aligned} \quad (\text{A4})$$

and the third derivatives are

$$\begin{aligned} \dddot{I}_{xy} = \dddot{M}_{xy} &= -\frac{3}{4}S^2\rho_0 \dddot{z}_s, & \dddot{I}_{yz} = \dddot{M}_{yz} &= -\frac{3}{4}Sb\rho_0(z_s^2)''' , \\ \dddot{I}_{xz} = \dddot{M}_{xz} &= -\frac{3}{4}Sa\rho_0(z_s^2)''' . \end{aligned} \quad (\text{A5})$$

The derivatives of diagonal components of the mass moments are

$$\begin{aligned} \dot{M}_{xx} &= -Sa^2\rho_0 \dot{z}_s, & \dot{M}_{yy} &= -Sb^2\rho_0 \dot{z}_s, & \dot{M}_{zz} &= -S\rho_0(z_s^3)', \\ \ddot{M}_{xx} &= -Sa^2\rho_0 \ddot{z}_s, & \ddot{M}_{yy} &= -Sb^2\rho_0 \ddot{z}_s, & \ddot{M}_{zz} &= -S\rho_0(z_s^3)'' , \\ \ddot{M}_{xx} &= -Sa^2\rho_0 \ddot{z}_s, & \ddot{M}_{yy} &= -Sb^2\rho_0 \ddot{z}_s, & \ddot{M}_{zz} &= -S\rho_0(z_s^3)'' . \end{aligned} \quad (\text{A6})$$

The derivatives of the trace of the mass moment are

$$\begin{aligned} (\text{Tr}M)' &= S\rho_0\{-(a^2 + b^2)\dot{z}_s - (z_s^3)'\}, \\ (\text{Tr}M)'' &= S\rho_0\{-(a^2 + b^2)\ddot{z}_s - (z_s^3)''\}, \\ (\text{Tr}M)''' &= S\rho_0\{-(a^2 + b^2)\dddot{z}_s - (z_s^3)'''\}. \end{aligned} \quad (\text{A7})$$

The derivatives of diagonal components of the quadrupole moment are

$$\begin{aligned} \dot{I}_{xx} &= -\frac{1}{3}S\rho_0\{(2a^2 - b^2)\dot{z}_s - (z_s^3)'\}, \\ \dot{I}_{yy} &= -\frac{1}{3}S\rho_0\{(2b^2 - a^2)\dot{z}_s - (z_s^3)'\}, \\ \dot{I}_{zz} &= \frac{1}{3}S\rho_0\{(a^2 + b^2)\dot{z}_s - 2(z_s^3)'\}, \end{aligned} \quad (\text{A8})$$

the second derivatives are

$$\begin{aligned} \ddot{I}_{xx} &= -\frac{1}{3}S\rho_0\{(2a^2 - b^2)\ddot{z}_s - (z_s^3)''\}, \\ \ddot{I}_{yy} &= -\frac{1}{3}S\rho_0\{(2b^2 - a^2)\ddot{z}_s - (z_s^3)''\}, \\ \ddot{I}_{zz} &= \frac{1}{3}S\rho_0\{(a^2 + b^2)\ddot{z}_s - 2(z_s^3)''\}, \end{aligned} \quad (\text{A9})$$

and third are

$$\begin{aligned} \dddot{I}_{xx} &= -\frac{1}{3}S\rho_0\{(2a^2 - b^2)\dddot{z}_s - (z_s^3)'''\}, \\ \dddot{I}_{yy} &= -\frac{1}{3}S\rho_0\{(2b^2 - a^2)\dddot{z}_s - (z_s^3)'''\}, \\ \dddot{I}_{zz} &= \frac{1}{3}S\rho_0\{(a^2 + b^2)\dddot{z}_s - 2(z_s^3)'''\}. \end{aligned} \quad (\text{A10})$$

When using the ansatz for the function  $z_s$  (39) some derivatives simplify significantly. Let us mention that to this point, we did not use the ansatz for  $z_s$  (39) and a every formula was derived for the general function of time  $z_s(t)$ . At this point in time, we are not aware of better ansatz for this function.

### 3. The derivatives of mass moment and quadrupole moment with substitution for $z_s$

The derivatives of the non-diagonal components of quadrupole moment read

$$\begin{aligned} \dot{I}_{xy} = \dot{M}_{xy} &= \frac{3}{4}S^2\rho_0 v_s, & \ddot{I}_{xy} = \ddot{M}_{xy} &= 0, \\ \dot{I}_{yz} = \dot{M}_{yz} &= \frac{3}{4}Sb\rho_0 v_s^2, & \ddot{I}_{yz} = \ddot{M}_{yz} &= 0, \\ \dot{I}_{xz} = \dot{M}_{xz} &= \frac{3}{4}Sa\rho_0 v_s^2, & \ddot{I}_{xz} = \ddot{M}_{xz} &= 0, \\ \ddot{I}_{xy} = \ddot{M}_{xy} &= 0, & \ddot{I}_{yz} = \ddot{M}_{yz} &= 0, & \ddot{I}_{xz} = \ddot{M}_{xz} &= 0, \end{aligned} \quad (\text{A11})$$

and diagonal components of the mass moment are

$$\begin{aligned} \dot{M}_{xx} &= Sa^2\rho_0 v_s, & \ddot{M}_{xx} = \ddot{M}_{xx} &= 0, \\ \dot{M}_{yy} &= Sb^2\rho_0 v_s, & \ddot{M}_{yy} = \ddot{M}_{yy} &= 0, \\ \dot{M}_{zz} &= 3S\rho_0 v_s(v_s^2 t^2 - 2v_s f_1 t + f_1^2), & \ddot{M}_{zz} &= 6S\rho_0 v_s^3, \\ \ddot{M}_{zz} &= 6S\rho_0 v_s^2(v_s t - f_1). \end{aligned} \quad (\text{A12})$$

The derivatives of the trace of the mass moment take the form,

$$\begin{aligned} (\text{Tr}M) &= S\rho_0 v_s \{3v_s^2 t^2 - 6v_s f_1 t + (a^2 + b^2 + 3f_1^2)\}, \\ (\text{Tr}M)'' &= 2S\rho_0 v_s^2 (3v_s t - f_1), \\ (\text{Tr}M)''' &= 6S\rho_0 v_s^3. \end{aligned} \quad (\text{A13})$$

The derivatives of diagonal components of the

quadrupole moment are

$$\begin{aligned} \dot{I}_{xx} &= \frac{1}{3} S\rho_0 v_s \{-3v_s^2 t^2 + 6v_s f_1 t + (2a^2 - b^2 - 3f_1^2)\}, \\ \dot{I}_{yy} &= \frac{1}{3} S\rho_0 v_s \{-3v_s^2 t^2 + 6v_s f_1 t + (2b^2 - a^2 - 3f_1^2)\}, \\ \dot{I}_{zz} &= \frac{1}{3} S\rho_0 v_s \{6v_s^2 t^2 - 12v_s f_1 t + (6f_1^2 - a^2 - b^2)\}, \end{aligned} \quad (\text{A14})$$

the second derivatives are

$$\begin{aligned} \ddot{I}_{xx} &= -2S\rho_0 v_s^2 (v_s t - f_1), \quad \ddot{I}_{yy} = -2S\rho_0 v_s^2 (v_s t - f_1), \\ \ddot{I}_{zz} &= 4S\rho_0 v_s^2 (v_s t - f_1), \end{aligned} \quad (\text{A15})$$

and third derivatives are

$$\dddot{I}_{xx} = -2S\rho_0 v_s^3, \quad \dddot{I}_{yy} = -2S\rho_0 v_s^3, \quad \dddot{I}_{zz} = 4S\rho_0 v_s^3. \quad (\text{A16})$$

- 
- [1] A. Einstein, Sitz. Preuss. Akad. Wiss. Berlin, 154 (1918).  
[2] B. P. Abbott *et al.*, Phys. Rev. Lett. **116**, 061102 (2016).  
[3] R. A. Hulse and J. H. Taylor, Astro. Phys. J **L51**, 195 (1975).  
[4] C. W. Misner, K. S. Thorne, and J. A. Wheeler, "Gravitation," (W. H. Freeman and Company, New York, 1973).  
[5] R. B. Jr., R. C. Woods, and F. Li, Proceedings of the Space Technology and Applications International Forum (STAIF-2006), edited by M. S. El-Genk **813**, 1280 (2006).  
[6] F.-Y. Li, H. Wen, and Z.-Y. Fang, Chin. Phys. B **22**, 120402 (2013).  
[7] F. Li, N. Yang, Z. Fang, R. M. L. Baker, G. V. Stephenson, and H. Wen, Phys. Rev. D **80**, 064013 (2009).  
[8] A. Arvanitaki and A. A. Geraci, Phys. Rev. Lett. **110**, 071105 (2013).  
[9] J. Weber, Phys. Rev. **117**, 306 (1960).  
[10] H. A. de Waard, L. Gottardi, J. van Houwelingen, A. Shumack, and G. Frossati, Classical Quantum Gravity **20**, S143 (2003).  
[11] <http://www.auriga.lnl.infn.it/>.  
[12] M. Cerdonio *et al.*, Classical Quantum Gravity **14**, 1491 (2003).  
[13] <http://www.ligo.org/>.  
[14] T. T. Fricke *et al.*, Classical Quantum Gravity **29**, 065005 (2012).  
[15] <http://www.cascina.virgo.infn.it/>.  
[16] V. B. Braginskij, Phys. Uspekhi **43**, 691 (2000).  
[17] <http://lisa.nasa.gov/>.  
[18] K. Yagi, Int. J. Mod. Phys. D **22**, 1341013 (2013).  
[19] <http://www.geo600.org/>.  
[20] K. Tang *et al.*, Radio Science Conference Proceedings, K30 (2004).  
[21] J. F. Chapline, Phys. Rev. D **10**, 1064 (1974).  
[22] V. N. Rudenko, Gravitation and Cosmology **10**, 41 (2004).  
[23] X. Ribeyre and V. T. Tikhonchuk, in *Proceedings 12th marcel grossmann Meeting on General Relativity (MG 12)*, Conference in Paris, 2009, Marcel Grossmann Series No. 17 (IcraIt, Paris, 2010) pp. 1640–1642.  
[24] X. Ribeyre and V. T. Tikhonchuk, in *Presentation on IZEST-ELI-NP Conference 2014 Paris*, IZEST – ELI-NP Conference in Paris, 2014 (IZEST, Paris, 2014).  
[25] <http://petal.aquitaine.fr/>.  
[26] <https://lasers.lnl.gov/science/photon-science/arc>.  
[27] <http://www.eli-beams.eu>.  
[28] R. Fabbro, C. Max, and E. Fabre, Phys. Fluids **25**, 5 (1984).  
[29] N. Naumova, T. Schlegel, V. T. Tikhonchuk, C. Labaune, I. V. Sokolov, and G. Mourou, Phys. Rev. Lett. **102**, 025002 (2009).  
[30] R. M. L. Baker and F. Y. Li, in *Proceedings of the Space Technology and Applications International Forum (STAIF-2005)*, STAIF, 2005, edited by M. S. El-Genk (America Institute of Physics, Melville, New York, 2005).  
[31] F. Li and R. Baker, Presentation on [www.gravwave.com](http://www.gravwave.com), Development of the Li-Baker ultra-high sensitivity high frequency relic gravitational wave detector (2011).  
[32] M. E. Gertsenshtein, J. Exp. Theor. Phys. (USSR) **41**, 113 (1961).  
[33] M. E. Gertsenshtein, Sov. Phys. JETP **14**, 84 (1962).  
[34] M. Maggiore, "Gravitational waves: Volume 1: Theory and experiments," (Oxford University Press, New York, 2008).  
[35] J. Bičák and V. N. Rudenko, "Theorie relativit a gravitan vlny," (Textbook, MFF UK, Prague, Prague, 1986).  
[36] S. Atzeni and J. Meyer-Ter-Vehn, "Physics of inertial fusion," (Clarendon Press-Oxford, Oxford, 2004).  
[37] <http://www.apollon-laser.fr/>.  
[38] <https://apri.gist.ac.kr/eng/>.  
[39] H. Azechi, J. Phys.: Conf. Series **112**, 012002 (2008).  
[40] D. N. Maywar, J. H. Kelly, L. J. Waxer, S. F. B. Morse, I. A. Begishev, J. Bromage, C. Dorrer, J. L. Edwards, L. Folsbee, and M. J. Guardalben, J. Phys.: Conf. Series **112** (2008).